POLITECNICO DI TORINO

Master's Degree in Physics of Complex Systems

Master's Thesis

Time irreversibility in a transitional boundary layer

Supervisors:
prof. Luca Ridolfi
prof.ssa Stefania Scarsoglio
prof. Giovanni Iacobello
(University of Surrey)

Candidate:
Miriana Galante

July 2025

Abstract

Laminar to turbulent flow transition is a complex phenomenon that is currently widely investigated in the field of fluid dynamics. In particular, the study of time irreversibility - intended as statistical asymmetry of signals under time reversal - of a transitional boundary layer can offer new perspectives in the analysis of turbulence and non-stationary processes. Therefore, the connection between the turbulent structure of the boundary layer and the irreversibility of the velocity signals is an important subject of research.

This thesis proposes a quantitative and point-to-point analysis of the time irreversibility of a transitional boundary layer and makes use of numerical data from the John Hopkins Turbulence Database (JHTDB), which simulate an incompressible flow on a flat plane subject to a bypass transition induced by isotropic turbulence at the inlet.

Time series of the velocity components u, v and w are transformed into graphs using different Visibility Graph methods, which are able to represent and study the geometric structure of signals using the tools of graph theory. Time irreversibility is quantified through the Kullback-Leibler divergence I_k of the ingoing and outgoing degree probability distributions of the nodes and measured by comparison with a reversible null model through its Z-Score $I_{k,r}$.

The results show that the regions exhibiting the highest levels of irreversibility are located in the transition zone and close to the wall and coincide with regions characterised by high turbulent fluctuations, particularly in the buffer layer. It is also observed that irreversibility does not depend directly on the amplitude of the fluctuations, rather it is influenced by their temporal asymmetry and by the

geometric structure of the signal. A local analysis by means of temporal windows suggests a correlation between irreversibility and the overlap regions between laminar and turbulent parts of the signal.

These results offer a new point of view on the interpretation of turbulent transition using graph theory, thereby providing a first step towards the understanding of time irreversibility and its connection to the turbulent structures of a boundary layer. Future studies may extend the analysis to the time-space dynamics of a single spot and its evolution along the plate, in order to unveil the mechanisms through which local asymmetries and coherent structures contribute to the global irreversibility of the flow.

Acknowledgements

I am deeply grateful to the professors that have followed the writing of this thesis. To professor Luca Ridolfi, whose support has been precious from day one and for his valuable advice during the most adverse moments, to professor Stefania Scarsoglio for the trust and support provided, and to professor Giovanni Iacobello, who has been a point of reference during my stay at University of Surrey, whose expertise has taught me a lot about science and research and whose passion has inspired me and nourished my hunger for learning.

These months have been extremely fruitful for the growth of my knowledge and for the improvement of my skills, from both a technical and personal point of view, thanks to you.

Contents

Chapter 1

Introduction

The transition from laminar to turbulent flow is a complex and intriguing phenomenon in fluid dynamics. Despite decades of research, many aspects of this process are still far from a complete theoretical understanding, especially when dealing with transitional boundary layers where both laminar and turbulent features coexist. The understanding of the dynamics of the transition is crucial not only for the theoretical development, but also for numerous physical and engineering applications.

In this framework, the study of time irreversibility is an additional topic of considerable interest, because it allows to acquire a deepen knowledge of the laminar to turbulent transition in boundary layers, but also to explore important properties of out-of-equilibrium systems. Turbulence, in fact, is an emblematic example of non-equilibrium systems, which are, by constitution, irreversible [1].

A reversible, or equivalently, irreversible, process is defined in terms of its statistics, that is, a dynamical process is reversible if its joint distribution does not change under time reversal [2, 3]. Reversible processes include, for instance, Gaussian linear processes, such as white noise, conservative chaotic processes, and in general all those processes related to thermodynamic equilibrium in stastistical physics [4, 5]. On the contrary, non-linear stochastic processes and dissipative chaotic processes are generally irreversible [4, 5] and associated to out-of-equilibrium systems in thermodynamics [6, 7, 8, 9, 10].

Turbulence is intrinsically irreversible because of the chaotic and strongly non linear processes that are involved in its development, such as the energy cascade

[11, 12]. Furthermore, in the presence of a wall bounded flow, even more degrees of complexity come into play, because of the different structures and motions [13, 14] that are induced in such setup and whose interactions become an additional cause of irreversibility.

Much of the current literature on irreversibility in turbulence focuses on homogeneous isotropic turbulence, often adopting a Lagrangian point of view [15, 16, 17], following the motion of fluid particles in the flow and revealing the connection between energy dissipation and time irreversibility [1]. The Eulerian framework has also been used and compared to the Langrangian one [16, 18], expanding the understanding of the phenomenon from multiple observational viewpoints. However, wall-bounded turbulence has only been recently investigated in this sense, exploring the complex dynamics given by the coherent structures that characterise a boundary layer and the inter-scale interactions [19, 20].

To address the challenge of getting a deeper understanding of wall-bounded turbulence, this thesis follows the line of a recent research [20], that adopted an Eulerian multiscale framework based on visibility graphs to analyse time series of the velocities of a turbulent boundary layer.

This graph-theoretical approach provides a powerful method to study complex time series by transforming them into networks that preserve the essential features of the original signals [21, 22]: all information is mapped from the time series to the graph according to a geometric criterion, creating a one-to-one ordered correspondence between the series data and the nodes of the graph [21].

This method has been previously applied to many study fields and widely used in non-linear time series analysis [4, 5, 23, 24, 25, 26, 27], and has proven to be capable of providing highly reliable and robust results, especially because it does not require any a priory parameter or any pre-processing simbolisation on the signals, but only the application of the geometric criterion.

The analysis has here been extended to the case of transitional boundary layers, a domain that has so far received limited attention in the literature. The focus is placed on the case of a bypass transition, which is characterised by the sudden onset of turbulence due to external disturbances on a previously completely laminar boundary layer [28, 13]. The analysis has been performed on data obtained from a

high-resolution numerical simulation of such scenario, publicly available through the Johns Hopkins Turbulence Database (JHTDB). The choice of a bypass transition offers a unique opportunity to investigate how coherent structures like streaks and turbulent spots contribute to the temporal asymmetry of the flow.

In the study, time irreversibility is eventually quantified in the visibility graph framework by comparing the in-going and out-going degree distributions of the graph nodes through the Kullback–Leibler divergence, and validated against a null model of reversible signals via its Z-score.

This work offers a new perspective on the nature of turbulent transition, showing that time irreversibility can serve as a signature of the underlying dynamics and perhaps as a tool for identifying and characterising transitional processes in complex flows. Although still in an exploratory phase, the approach adopted here opens new perspectives to more refined analyses.

The thesis is structured as follows. Chapter 2 provides an overview on the concepts of time irreversibility in turbulence and on the structure of transitional boundary layers. Chapter 3 presents the dataset, the pre-processing steps, and the visibility graph methodology. Chapter 4 introduces basic statistical analyses to identify the transitional zone. Chapter 5 discusses the main results, including global and local measurements of irreversibility and their interpretation. Finally, Chapter 6 draws the conclusions and suggests directions for future research.

Chapter 2

Time irreversibility

2.1 Time irreversibility in turbulence

The dynamics of a fluid are governed by the Navier-Stokes (N-S) equations

$$\frac{Du}{Dt} = -\frac{1}{\rho}\nabla p + \nu\nabla^2 u$$

where $Du/Dt = \partial_t u + u\nabla u$ is the material derivative of the velocity field, p is the pressure and ν the kinematic viscosity. In the absence of viscosity the Euler equation is recovered:

$$\frac{Du}{Dt} = -\frac{1}{\rho}\nabla p$$

The description of fluid motion is based on the competition between the inertia of the fluid and the diffusion of momentum by viscosity [1], which is encoded into the Reynolds number

$$Re = \frac{U_L L}{\nu}$$

where L is the characteristic length of the flow and U_L the associated velocity.

It is the inertial effect that leads the flow towards instability, while the viscosity drives a damping effect. Hence, turbulent flows are characterised by high Reynolds number, with the predominancy of inertia, and develop irregular and strong variations of the velocity.

Fully developed turbulent flows are well described by the Euler equation [29], when at large scales viscous effects are negligible ($\nu \to 0$) and only inertial forces

drive the dynamics ($Re \to \infty$). This equation is invariant under reversal of time and hence time reversible. In fact, if considering the transformation $t \to -t$ and $u \to -u$, none of its terms is affected.

Conversely, the N-S are not invariant under time reversal, because of the viscous term that changes sign and explicitly breaks their time-reversal symmetry. Nonetheless, turbulent flows are not reversible, even if characterised by very high Reynolds numbers. This is due to the fact that the flow is maintained turbulent by a constant supply of kinetic energy and continously dissipates it via the process of energy cascade.

Turbulent motion can be interpreted in terms of an energy cascade [30] through a vast interval of scales. In fact, it is a property of turbulent flows that the scales at which energy is supplied are very different from those at which it is dissipated [1]: if turbulence is considered as made of eddies[1] of different sizes, the largest ones are comparable to the flow scale with velocity comparable to the characteristic velocity [12].

The energy cascade, that is, the transfer of energy, starts because large eddies are unstable and break up, and move energy to smaller eddies, which are still unstable and in turn transfer energy to even smaller eddies, in an out-of-equilibrium process. This flux of energy goes on until the size of the eddy is sufficiently small - of the Kolmogorov scale η [11] -, with a small Reynolds number such that viscosity is dominant and dissipates the kinetic energy[2].

The rate of energy transfer from the large scales remains constant throughout the intermediate inertial subrange, that is, from the energy production range up to the dissipation range, and defines also the dissipation rate ε. In practice, energy is dissipated even for high Reynolds numbers, with ε independent of the viscosity ν. This is what is called anomalous dissipation [11] and spontaneously breaks the time-reversal symmetry associated to large Reynolds number flows, making the energy flux irreversible [18].

In summary, turbulence is an out-of-equilibrium, and therefore an irreversible,

[1]The definition is not precise, but it can be considered as a turbulent motion of size l, coherent in this region [12], or as a swirling movement that deviates from the general flow of the fluid.

[2]This is valid for 3D turbulence. In the case of 2D turbulence the process is the inverse and it is called inverse energy cascade, from small to large scales [1, 16, 29].

system, because of the energy flux from large to small scales that is the cause of the spontaneous time-reversal symmetry breaking and is due to the nonlinear terms of the N-S equations, which are formally symmetric (except for the viscous term). On the other side, the dissipative term of the equations represent an explicit symmetry breaking and allows to distinguish between the intrinsic irreversibility, imposed by the viscous dissipation, and the statistical irreversibility, deriving from the collective, chaotic behaviour of complex systems, even if the underlying laws are reversible over time [29].

It is natural, being the aim of this work, to focus the attention on the case of boundary layers when invested by turbulence. Boundary layers form when a viscous stream flows over a solid surface, creating a region with strong shear. The behaviour of the flow can vary, from being completely laminar to completely turbulent, passing through states of strong intermittency.

Boundary layers present a layered structure: a viscous sublayer, the buffer layer and an outer layer dominated by inertia, that interact dynamically [12]. In particular, during the transition, the boundary layer is characterised by the presence of coherent structures, such as streaks or vortices, which are organised along these regions, interacting with each other in non-linear ways and creating turbulent spots.

This is the reason why these flows are particularly interesting for the study of irreversibility: in fact, the interaction between these coherent structures induced by the wall and the evolution of turbulence add a further level of complexity [20] to the investigation of the symmetry breaking.

Studying time irreversibility within boundary layers in transition could be a starting point to understand how temporal asymmetry emerges in complex systems out of equilibrium, even in the absence of dominant dissipation.

2.2 Transitional boundary layer

Within the fascinating and complex study of turbulence, there are several ways for a flow to transition from laminar to turbulent, for instance via Tollmien-Schlichting instability waves, cross-flow instabilities, Görtler instabilities and many others [13].

When it comes to boundary layer with zero pressure gradient, the two main routes to transition are the orderly transition and the bypass transition. The former is briefly introduced, while the latter is examined in depth, since it constitutes the

primary focus of the present thesis, as the available data are obtained from a simulation specifically reproducing a bypass transition scenario.

2.2.1 Orderly transition

Orderly transition to turbulence is a gradual process and usually passes through three different stages: receptivity, linear instability and non-linear breakdown.

1. Receptivity: Transition process start with the receptivity from the boundary layer, that is, its response to (not too high) environmental disturbances such as acoustic waves, vortical perturbations, vibrational fluctuations and so on. Their interaction with leading edge of the boundary layer causes the generation of instability waves, like the Tollmien-Schlichting waves, in a region of low local Reynolds number [31]. In this case the transition to turbulence is a slow process, since these waves are weakly unstable because of viscous mechanisms [28].

2. Linear instability: If the flow is sufficiently unstable, the T-S bidimensional waves grow exponentially as described by linear stability theory (a brief description of such theory is given in Appendix A). Then secondary tridimensional instabilities are activated because of nonlinear interactions between waves, through different mechanisms (K-type, N-type, etc... [31]). In this phase different structures like streamwise vortices or peak and valleys are observed.

3. Non-linear breakdown: When perturbations' amplitude reach 1-2% of the free-stream velocity the flow collapses in a non linear breakdown, transitioning to turbulence through a randomisation phase and through the creation of coherent tridimensional structures. In this phase turbulent spots, small localised chaotic regions of turbulence, are generated. Then they spread throughout the surface and progressively merge in a fully turbulent region.

A schematic picture of the phenomenon is shown in figure 2.1.

Between the creation of the first turbulent spots and the establishment of turbulence, the boundary layer presents a transition zone, a region characterised by high levels of intermittency, that is, the random alternation of laminar and turbulent areas, described by the variable γ, the fraction of time in which the flow is turbulent [32].

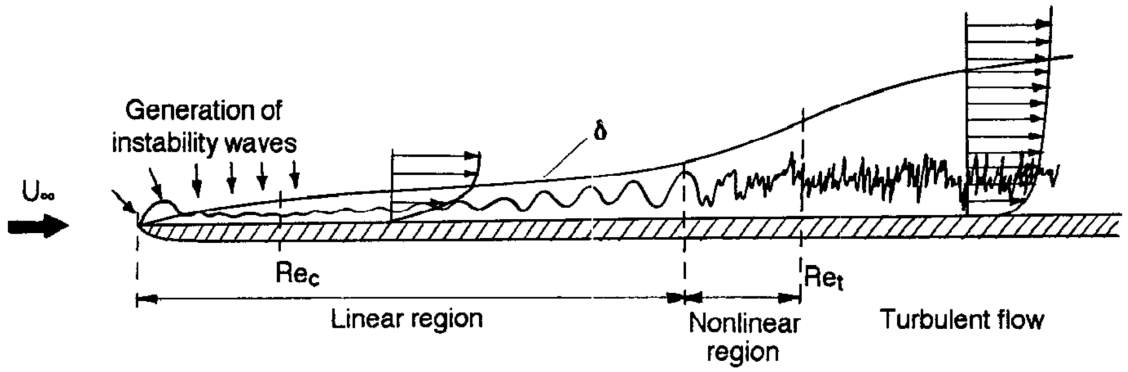

Figure 2.1: Schematic picture of the orderly transition to turbulence. Instability waves are generated at low Reynolds numbers by external disturbances. Then they amplify linearly and non-linearly until the breakdown into a turbulent flow. Image reproduced from Kachanov, 1994 [31].

2.2.2 Bypass transition

Bypass transition takes place when a laminar boundary layer is exposed to free-stream turbulence with intensity of order 1% or more [28]. The term bypass is representative of the fact that the transition bypasses the preliminary phase of Tollmien-Schlichting instability waves, with a much faster process. However, the stochastic and sporadic nature of the onset of turbulence makes it a quite complicated process to be studied, and often necessitates deep investigation by means of techniques capable to discriminate turbulent regions from laminar ones [13].

It is commonly described as a multi-stage process:

1. Shear sheltering of high frequency perturbations.
2. Generation of elongated distorsions of the velocity, the streaks.
3. Amplification of the streaks.
4. Secondary instability of the streaks.
5. Breakdown into turbulent spots.
6. Merging of the spots.

When free-stream vortical turbulence invest a laminar boundary layer, not all perturbations are able to penetrate it.

The shear flow, in fact, works as a filter and shelters high frequency components of the free-stream disturbances, allowing, at finite Reynolds numbers (much lower than those predicted by linear stability theory [33]), only low frequency ones to enter the boundary layer locally, not only at the leading edge.

This leads to the formation of velocity perturbations that are are dominated by the streamwise velocity component and are elongated in this direction by rapid distorsion mechanisms [28], forming the so-called streaks[3]. Meanwhile, the turbulence in the free-stream decays while being convected downstream [13], as it can be seen in figure 2.2.

The low frequency modes that penetrate the boundary layer are generated by viscously decaying free-stream turbulence and cannot lead directly to instability [35]. However, in the presence of shear - that is, a velocity gradient in the wall-normal direction - a small cross-stream disturbance can advect the mean velocity upward or downward, even in the absence of an inflection point (as required by Rayleigh's criterion for classical instability [36]). This vertical transport modifies the local streamwise velocity: low-speed fluid is lifted away from the wall, while high-speed fluid is pushed downward creating elongated streaks in the streamwise velocity. This is what is called the lift-up effect [37]. The result is the formation of alternating high- and low-speed streaks in the spanwise direction [38].

In particular, the most intense low-speed streaks, also called backward jets [39], play a crucial role in initiating the transition, as they locally reduce the streamwise velocity below the mean and can act as receptivity sites for incoming free-stream disturbances.

While such jets exist throughout the boundary layer, they are able to couple with small-scale free-stream turbulence only when upwelling motions lift them toward the upper portion of the boundary layer [28].

There, they become receptive to external disturbances and act as initiators of localized instabilities by creating new three-dimensional, low-frequency structures

[3]The streaks are also named Klebanoff modes [34], not in the sense that they are eigenfunctions of a response equation, but because they can be Fourier-decomposed and are coherently organized in space. In fact, their maximum growth is defined for a limited range of spanwise wavenumbers and this allow to create the streaky structure in this direction. Furthermore, their growth is not exponential in time - as usual modal instabilities - but is linear due to the lift-up effect.

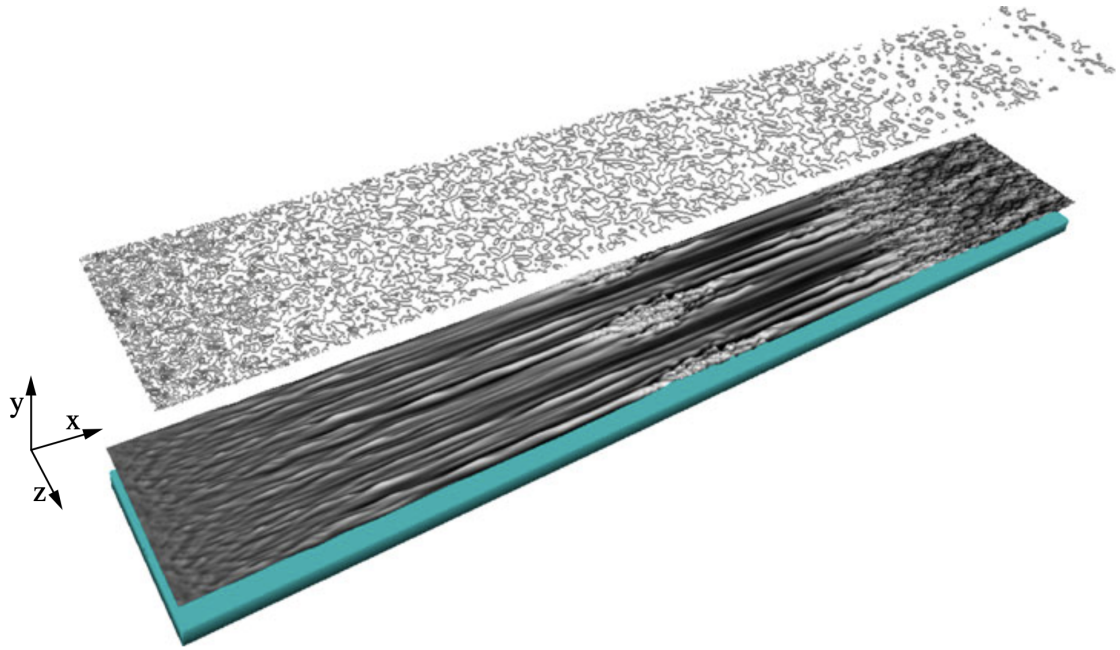

Figure 2.2: Contours of the streamwise velocity perturbation for a plane in the boundary layer (down) and a plane in the free-stream (up). The free-stream turbulence decays while convected downstream. Inside the boundary layer elongated structures (streaks) are evident upstream the plate, then some turbulent spots appear, and finally downstream the complete turbulent boundary layer. Image reproduced from Zaki, 2013 [13].

that again can overcome the shear sheltering effect at the border of the boundary layer.

After the lift up, the flow is in a more complicated laminar state characterised by nonlinear interaction. The streaks grow linearly with the boundary layer thickness over time, reaching very high amplitudes, from 10% to 25% of the mean flow speed, depending on the intensity of the free-stream turbulence.

The streaks are constantly being perturbed by external turbulence, nonetheless, instability events are rare[4] and most perturbations remain subcritical or decay [38].

[4]Only streaks with highest amplitude generate breakdown to turbulence. This is why it is important to study them by considering the amplitudes distribution, rather than mean values of the fluctuations, such as u_{rms}, that could hide rare events in the tails of the distribution [13].

But when their amplitude increases up to a sufficiently high value, they can trigger secondary instabilities by distorting the local streamwise velocity and introducing new inflection points in both the wall-normal and spanwise velocity profile [40, 41].

The secondary instabilities generates oscillations of the streaks, both symmetric and antisymmetric, that break the streak coherence and lead to the formation of localised turbulent spots, which are already developed regions of turbulence and the transition mechanism is already well underway [28].

The majority of the spots originate near the top of the boundary layer, being generated by free-stream eddies, and afterwards cascade towards the wall. Once these patches of irregular motion are formed, they spread and fill the boundary layer, getting more and more intense as they propagate downstream. At some point they start to merge, forming juxtaposed zones of turbulent and laminar flow, just upstream of a fully turbulent region.

Eventually they all join in a main turbulent area which will grow until forming a fully turbulent region downstream the boundary layer.[28]

A schematic picture of the bypass transition is depicted in figure 2.3.

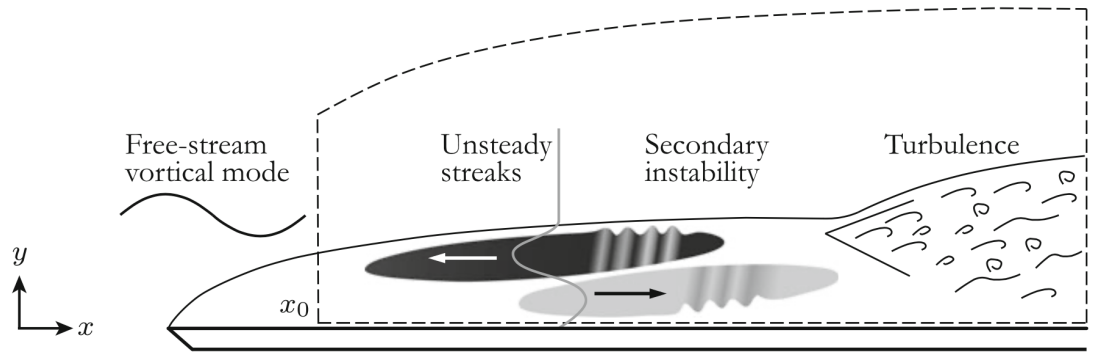

Figure 2.3: Schematic picture of the bypass transition to turbulence. Free-stream vortical turbulence enters the boundary layer by shear sheltering, longitudinal streamwise streaks are generated and amplify along the boundary layer, activating secondary instabilities that will lead to turbulence through the formation of turbulent spots. Image reproduced from Zaki, 2013 [13].

In this case it is possible to define three regions relevant to describe the transition: the buffeted laminar boundary layer, where the streaks develop amplified by

the shear; the region of intermittent turbulent spot formation - the transition zone - where secondary instabilities and spots evolve; and the fully turbulent boundary layer.

Chapter 3

Data and methods

3.1 The database

The data used in this study have been obtained from the John Hopkins Turbulence Database (JHTDB), an open numerical turbulence laboratory developed by the John Hopkins University and sponsored by the National Science Foundation. The database consists of several types of turbulence datasets produced via direct numerical simulations (DNS), including the transitional boundary layer one [42].

Simulations for the transitional boundary layer have been performed on an incompressible flow over a flat plate with an elliptical leading edge, in a zero-pressure gradient environment and imposing no slip condition at the wall.

Using streamwise, wall-normal and spanwise coordinates x, y, z for the system, the measures of the plate are $(1050 \times 240)L$, with respect to its half thickness L.

The inflow condition at the leading edge of the plate is given by the superposition of the uniform free stream velocity U_∞ (also used as reference velocity) and turbulent fluctuations u' simulated from a homogeneous isotropic turbulence in a periodic domain of size $(240 \times 15 \times 240)L$ rotated around z by an angle α.

The length scale of the inflow turbulence is $L_k = 1.8L$ and its intensity is $Tu = 3\%$ at the beginning of the plate; then it decays as it is advected downstream as $(x - x_g)^{-0.8}$ reaching less than $Tu = 0.5\%$ at the exit of the domain. The interaction of the turbulent fluctuations with the laminar boundary layer leads to the bypass transition to a fully turbulent boundary layer.

The Reynolds number based on the reference velocity and length and on the viscosity is $Re_L = U_\infty L/\nu = 800$.

The database domain actually comprehends only the rectangular domain after the leading edge of lengths $L_x \times L_y \times L_z = (969.8465 \times 26.4844 \times 240)L$, which corresponds to the coordinates

$$x \in [30.2185,1000.065]L,\ y \in [0.0036,26.4880]L,\ z \in [0,240]L.$$

At the database inlet the turbulence intensity is $Tu = 2.86\%$. A sketch of the domain with the reference frame is shown in figure 3.1.

The central point of the transition is supposed to be located around the value $x \approx 350L$, given a change in the growth of the curve $u = 0.99U_\infty$, a measure of the boundary layer thickness, and an abrupt change in the vertical velocity, which becomes negative as it is required by continuity to effect the change in the profile of the velocity from laminar to turbulent flow [42].

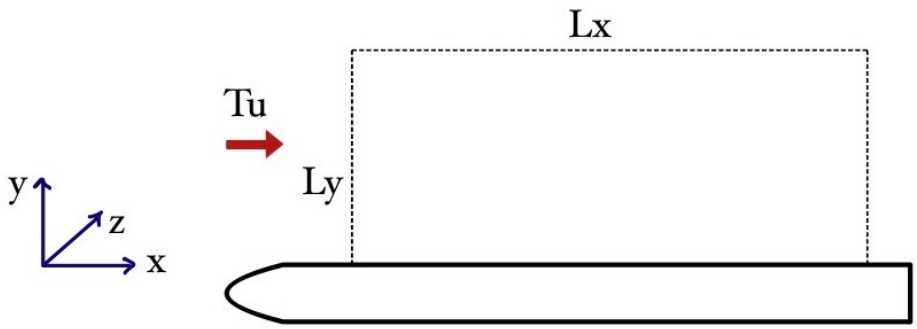

Figure 3.1: Schematic representation of the computational domain on a flat plate. The figure shows a side view of the domain, with length L_x and height L_y. The inlet flow has a turbulence level defined as Tu, indicated by the red arrow. The Cartesian reference system adopted is shown in the lower left-hand corner, with the x axis oriented along the main flow direction, the y axis oriented upwards and the z axis exiting the plane.

The domain grid counts $N_x \times N_y \times N_z = 3320 \times 224 \times 2048$ points, staggered along x and z with $\Delta x^+ = 11.9$ and $\Delta z^+ = 4.07$, while along y the grid spacing is irregular with a $\Delta y^+_{min} = 0.124$ close to the wall and with a grid stretching less than 3%.

The simulation time-step is $0.005L/U_\infty$, but snapshots have been saved in the dataset every $\Delta t = 0.25L/U_\infty$ for a total of 4701 snapshots along a total time of $1175L/U_\infty$.

The parameters' values used in the simulations are: $U_\infty = 1$, $L = 1$, $\nu = 1.25 \times 10^{-3}$. The database also provides some flow statistics averaged in z and t, such as the boundary layer thickness $\delta_{99} = (0.9648 - 15.0433)L$, the momentum thickness $\theta = (0.1318 - 1.8775)L$, and the Reynolds numbers $Re_\delta \equiv U_\infty \delta_{99}/\nu = (772 - 12035)$ and $Re_\theta \equiv U_\infty \theta/\nu = (105.5 - 1502.0)$.

The data that have been queried and used in the following are the velocity components u, v, w, respectively the streamwise, wall-normal, and spanwise components of the velocity of the flow.

3.2 Visualizing the time series

The velocities have been queried in the form of time-series of length 4701 time-steps, in order to be able to apply the visibility graph method to investigate the time irreversibility of the system.

Given the large number of points in the domain ($N_x \times N_y \times N_z$), each of them corresponding to a different time-series, a preliminary analysis has been carried out on a few points to begin with the understanding of the problem.

To give an idea of the evolution of the turbulence from a laminar flow to a completely turbulent one, some ideally significant points can be along the x domain 1, 597, 1097, 1951 and 3300, corresponding to the coordinates $x/L = 30.2185$, $x/L = 204.3759$, $x/L = 350.4812$ (approximately the center of the transition zone), $x/L = 600.0289$, $x/L = 994.2208$.

Here, in particular, at fixed $z/L = 0$, the wall normal positions $y/L = 0.4058$, $y/L = 1.0026$ e $y/L = 5.1266$, are considered.

In the first row of figure 3.2, at $y/L = 0.4058$, position that corresponds to the peak of the turbulent fluctuations, very close to the wall, the signal presents a small

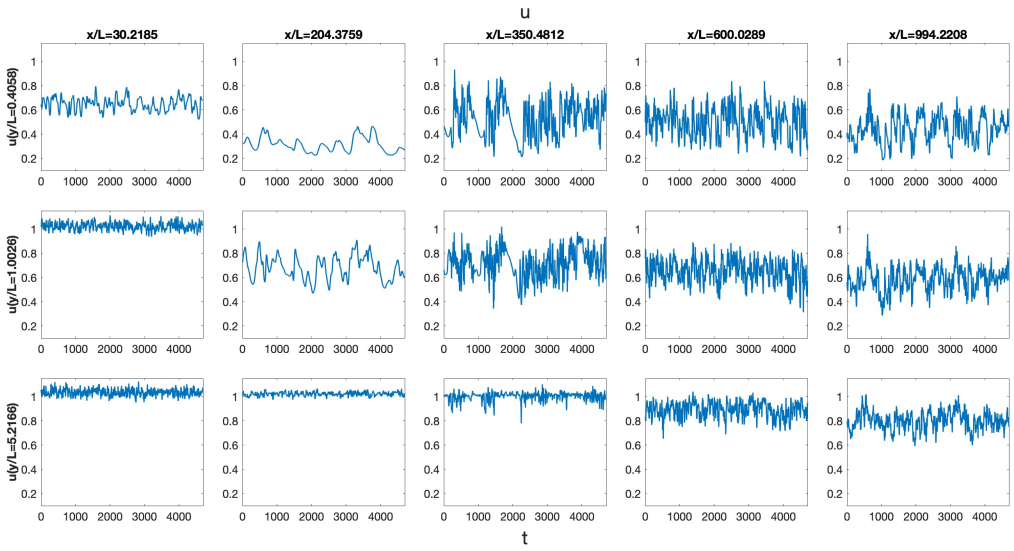

Figure 3.2: Time series of the u component of the velocity at different points of the domain, considering 5 positions along x and 3 along y, that highlight the evolution of the signals.

amplitude at the beginning of the domain, followed by a lower and almost constant velocity at the beginning of the transition zone, and then increasing in amplitude from the center of the zone onwards; as x increases, the velocity values decrease slightly, but maintain the turbulent fluctuations. Thus we see the transition from laminar to turbulent flow.

Signals belonging to the transition zone exhibit a big level of intermittency, alternating laminar and turbulent behaviour along time. They are characterised by the presence of turbulent spots, localised turbulent zones caused by the primary instabilities of the flow, that propagates downstream and spread spanwise. They mark the transition and as they grow while evolving in the flow, they join forming signals highly intermittent and completely turbulent.

Moving away from the wall, as y increases, this same behaviour appears but scaled down, with a signal at first laminar evolving into turbulent with x; consistently with the increasing boundary layer thickness, this occurs from larger x if sufficiently far from the wall.

In the normal and transversal directions (figures 3.3 and 3.4) all signals are on average null, but also in this case the signal is evidently larger in the center of the transition zone, where the flow begins to be turbulent, and near the wall.

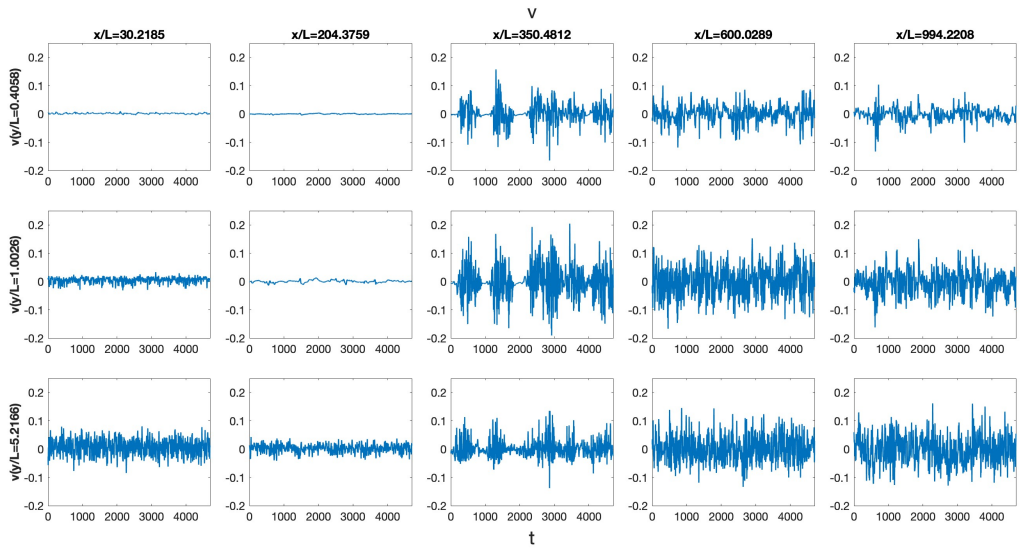

Figure 3.3: Time series of the v component of the velocity at different points of the domain, considering 5 positions along x and 3 along y, that highlight the evolution of the signals.

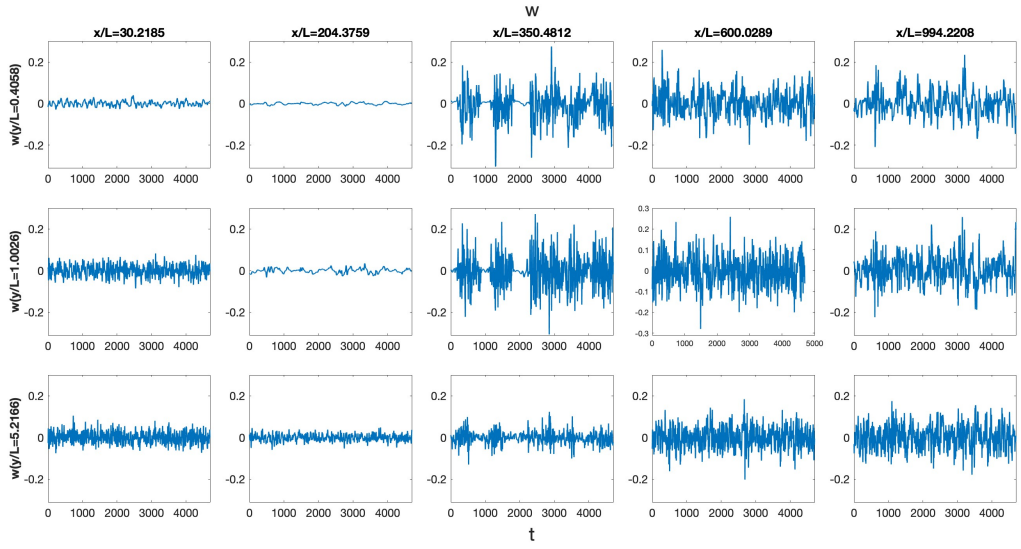

Figure 3.4: Time series of the w component of the velocity at different points of the domain, considering 5 positions along x and 3 along y, that highlight the evolution of the signals.

Moving away from it, the amplitude of the signals decreases. Again, the effect of the homogeneous turbulence arriving on the plate at $x/L = 30.2185$ is visible.

As far as these two components are concerned the most relevant y-position is the second one, as their peaks are located around $y/L \simeq 1$, but for completeness the other signals are also displayed.

3.3 Visibility graph method

The visibility graph methods represent a useful tool which can be used to fill the gap between nonlinear time series analysis and graph theory [4]. The method consists in an algorithm [43, 44] able to transform time series into graphs, which will inherit the main properties and characteristics of the series, allowing one to study them using complex network techniques. It can be proved that the topology of the graph conserves the structure of the time series [21].

All information is mapped from the time series to the graph according to a geometric criterion, creating a one-to-one ordered correspondence between the series data $\{x_t\}_{t=1,\dots,N}$ and the nodes of the graph [21].

3.3.1 The Natural Visibility Graph (NVG)

The more general version is encoded in the Natural Visibility Graph (NVG), where two nodes i and j - corresponding to series data x_i and x_j - will be connected by an edge if they are mutually visible, that is, if one can draw a straight line connecting them without intersecting any other intermediate node k, $i < k < j$.

Mathematically, visibility can be expressed through a convexity criterion: nodes i and j are connected if

$$x_k < x_i + \frac{k-i}{j-i}(x_j - x_i),\ \forall k : i < k < j$$

An example is depicted in figure 3.5: each point of the time series correspond to a node, which is connected to other visible nodes. In this particular case, the time series is periodic and so is its visibility graph, confirming the previously stated fact that the structure of the series is conserved in the topology of the graph.

The network can be represented by the adjacency matrix A, with entries

$$A_{ij} = \begin{cases} 1 & \text{if the criterion is satisfied} \\ 0 & \text{otherwise} \end{cases}$$

With this definition and being the connections undirected and unweighted, the adjacency matrix is binary and symmetrical.

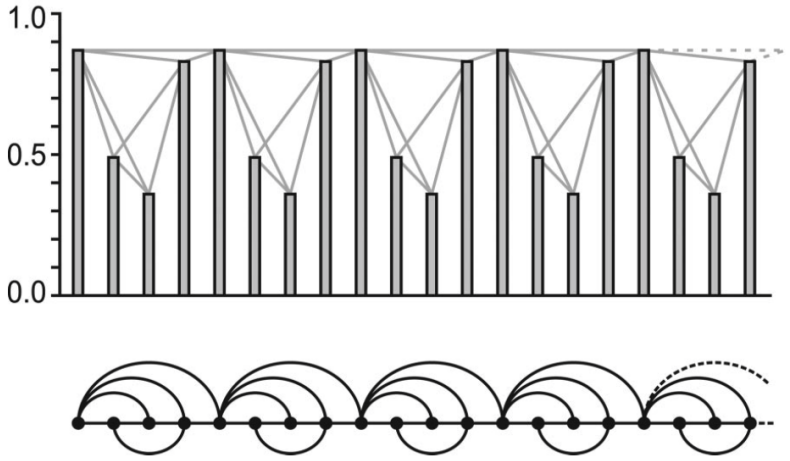

Figure 3.5: Example of a Natural Visibility Graph constructed from a periodic time series. To each point of the time series correspond a node in the graph, which conserves the series' structure. Image reproduced from Lacasa et al., 2008 [21].

The graph resulting from the mapping will always be connected (the two neighbours of a node are always visible), undirected and invariant under affine transformation of the series data such as translations and rescaling of the axes, as shown in figure 3.6. This invariance implies that different series may be described by the same visibility graph and adjacency matrix, hence some information about the series gets lost in the mapping.

A problem of this kind can be easily circumvented by generalising the method with the use of weighted networks, where a weight on the edge of the graph represent the slope of the visibility line connecting the data [21, 22]. This would also make the transformation series-graph reversible.

Visibility graphs have a natural order induced by the ordered time structure of the series that determines them [5]. If one defines the degree of a node $k(t)$ as the number of links a certain node has with other nodes, it becomes natural to define the degree sequence of the graph $\{k(t)\}_{t=1}^{N}$. Making a distinction on this definition can provide directionality to the network, allowing to create a directed version of the graph in terms of the temporal direction. This is done by distinguishing between the number of nodes that can see a given node from the number of nodes that a given

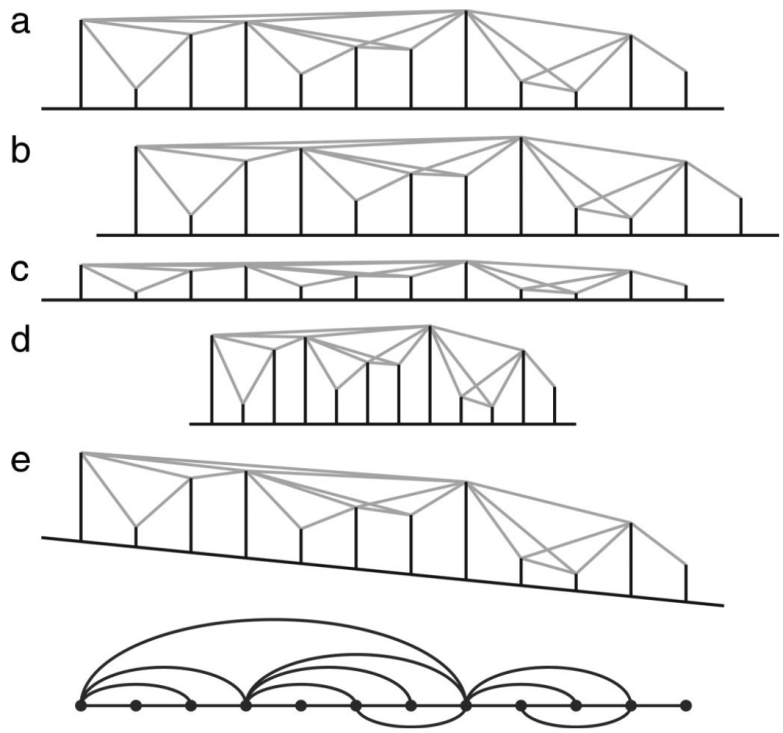

Figure 3.6: Example of invariance of the visibility graph under transformations of the time series. (a) Original time series with the connections between visible nodes. (b) Translation. (c) Vertical rescaling. (d) Horizontal rescaling. (e) Addition of a linear trend to the data. Image reproduced from Lacasa et al., 2008 [21].

node can see, and by creating two sequences $\{k_{in}(t)\}_{t=1}^{N}$ and $\{k_{out}(t)\}_{t=1}^{N}$, hence defining for node i an ingoing degree k_{in} and outgoing degree k_{out}, respectively, such that $k = k_{in} + k_{out}$.

The main important feature of visibility graphs is that, unlike other methods [9, 45, 46, 47, 48] often used in the analysis of time series, it does not require any a priory parameter or any pre-processing simbolisation, but only the application of the convexity criterion, which uses information from the whole series and makes the method reliable and robust [23, 49, 19, 20].

3.3.2 The Horizontal Visibility Graph (HVG)

The Horizontal Visibility Graph is a subclass of the Natural Visibility Graph, in which the time series data $\{x_t\}_{t=1,\ldots,N}$ are mapped into the nodes of the graph and are connected by horizontal lines. An edge between two nodes is created if the

following simpler criterium is satisfied:

$$x_k < \inf(x_i, x_j), \forall k : i < k < j$$

which means that one can draw an horizontal line between i and j without intersecting any intermediate datum x_k [22]. It is straightforward to see that HVGs are a subgraph of VGs and that they are outerplanar graphs [5]. In figure 3.7 an example of Horizontal Visibility Graph is displayed on the right, compared to the Natural Visibility Graph of the same time series, on the left.

Clearly, this algorithm is characterised by less visibility with respect to the previous case, due to the restrictions on the visibility given by its geometric criterion. This will cause the method to provide less statistics quantitatively speaking, but the quality of its features are not affected by this fact [22].

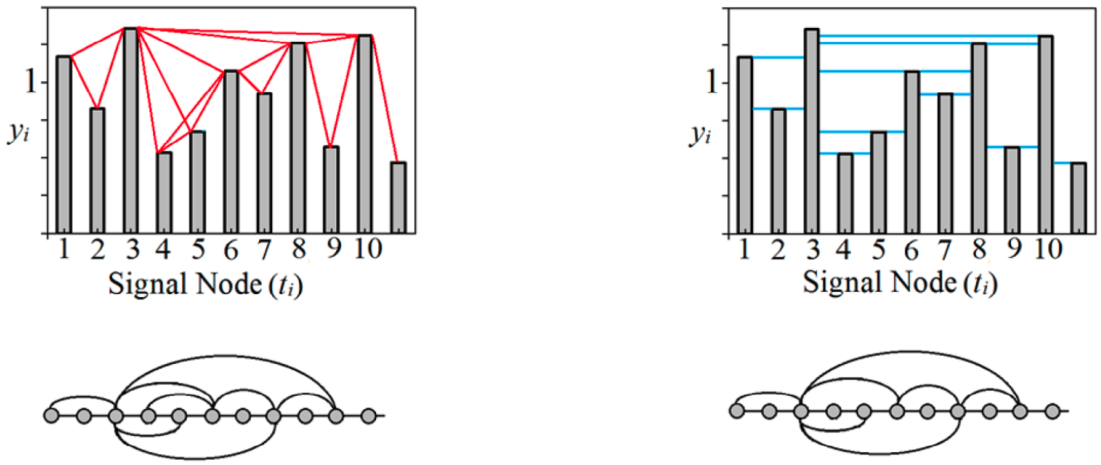

Figure 3.7: Comparison of a Natural Visibility Graph (left) and Horizontal Visibility Graph (right) of the same time series. It is evident that the HVG is a subgraph of the NVG, holding only some of its links. Image reproduced from Ahmadi et al., 2018 [50].

Both the NVG and HVG are effective in representing the time series and capturing its most important features, including irreversibility, with more or less accuracy depending on the models in analysis and on the typology of the signals [5].

Despite that, in the study of irreversibility, the main objective of the present work, it has been chosen to focus primarily on the use of HVG due its slightly easier implementation and some results will be compared with the NVG version for a more complete overview.

3.3.3 Irreversibility

Before defining how the irreversibility analysis of a time series works, it is necessary to exploit what being time reversible means.

A stationary time series $S = \{x_1, ..., x_n\}$ is statistically time reversible if it has the same joint probability distribution of its time reversed version $S^* = \{x_n, ..., x_1\}$, $\forall n$, that is, the two time series are equally probable [2, 3].

As already mentioned, the previously defined degree sequence of the graph $\{k(t)\}_{t=1}^{N}$, representing the sequence of number of connections of each node, can be split into two sequences $\{k_{in}(t)\}_{t=1}^{N}$ and $\{k_{out}(t)\}_{t=1}^{N}$ for the ingoing and outgoing degrees. These sequences are characterised by the important property that they are interchangeable under time series reversal [5], that is

$$k_{in}(t)[S] = k_{out}(t)[S^*], \quad k_{out}(t)[S] = k_{in}(t)[S^*].$$

Figure 3.8 reports an example of a directed Horizontal Visibility Graph, highlighting the difference between the ingoing and outgoing links in the series, which correspond to different values of k_{in} and k_{out} in the graph.

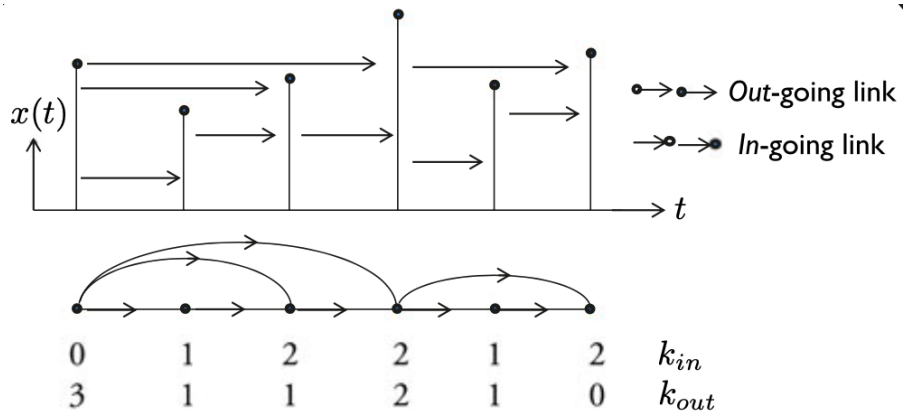

Figure 3.8: Example of a directed Horizontal Visibility Graph (below) and its corresponding time series (above), in which the visibility connections follow the temporal direction, distinguishing between ingoing and outgoing links. A different value of k_{in} and k_{out} correspond to each node of the graph. Image reproduced by Lacasa et al., 2012 [4].

The time irreversibility associated to a certain time series can be then measured by considering the distance between the probability distributions of the ingoing and

outgoing degrees, defined as $P_{out}(k) \equiv P(k_{out} = k)$ and $P_{in}(k) \equiv P(k_{in} = k)$ [4], which also share the previous property

$$P_{in}(k)[S] = P_{out}(k)[S^*],\ P_{out}(k)[S] = P_{in}(k)[S^*].$$

The distance between probability distributions can be calculated by means of the Kullback-Leibler divergence (KLD), which quantifies how different two distributions are and is a measure of relative entropy.

It is then possible to define irreversibility as

$$I_k = D[P_{out}(k)||P_{in}(k)] = \sum_k P_{out}(k)\ log\frac{P_{out}(k)}{P_{in}(k)}$$

and it vanishes if the two distributions coincide, hence when the time series is reversible, while it increases the more they are distant, quantifying time-series' irreversibility.

The choice of the KLD is motivated by its statistical significance. In fact, for the Chernoff-Stein lemma it represents the exponential error rate associated to hypothesis tests to distinguish two probability distributions, as the error tends to $e^{-ND(p||q)}$ for $N \to \infty$, or in other words the probability to incorrectly discern the distributions decreases the larger the KLD is [4]. Furthermore, in statistical mechanics the KLD is related to the thermodynamic entropy that a non equilibrium system is producing and it is hence able to provide information about the time irreversibility of the process that generates the data [6, 7, 8, 10].

Actually, even in the presence of truly reversible processes, the KLD may provide positive finite values for finite-size series and they will vanish as $N^{-\delta}$ as $N \to \infty$, being null only asymptotically. That is why reversibility is redefined as:

$$\lim_{N\to\infty} D[P_{out}(k)||P_{in}(k)] = 0$$

and truly irreversible processes will display positive value even in the limit of large N [5, 51]. Nevertheless, being the convergence quite slow, finite-size values can be used statistically to compare irreversibility values for finite samples as it happens in empirical datasets like the one used in this study.

As a final remark, the irreversibility calculation based on visibility graphs not only determine wether a time series is time reversible or irreversible, but it is also able to quantify the amount of irreversibility [4].

3.3.4 Irreversibility ratio

As it has been said previously, finite-size time series can result in positive values of the KLD even in the presence of reversible processes and this can cause some interpretability problems to the study of irreversibility.

To solve this issue a confidence index can be introduced [51]. It is calculated by applying a standardisation with respect to a null model, to see how much a sample differs from what it would be expected by a truly reversible process. The index is defined as the Z-Score of I_k:

$$I_{k,r} = \frac{I_k - \mu_{k,r}}{\sigma_{k,r}}$$

where $\mu_{k,r}$ is the mean on the null model, built by taking a certain number of randomisations [1] of the time series obtained by shuffling the original series and by computing the KLD on each of them, and $\sigma_{k,r}$ is their standard deviation. This formula expresses mathematically the idea of the distance of the series from its null reversible model, in standard deviations units.

In fact, for reversible processes both I_k and its null model value are expected to follow the same trend for increasing N, that is they should both tend to zero, and the irreversibility ratio should remain below 1, regardless of N.

Conversely, for irreversible processes, I_k is consistently greater than zero and stays positive even as N increases, while its null model, again, decreases with N, letting the irreversibility ratio increase with N. This means that for irreversible processes the time series length actively affects this measure.

However, generally speaking, after a certain threshold (which can be set to a value $O(1)$ or $O(10)$), the signal can be considered irreversible [51].

[1] Uncorrelated random series are reversible as demonstrated in Theorem 1 in [4].

Chapter 4

Preliminary analyses

4.1 Identification of the transitional zone

A first necessary step to investigate the transitional boundary layer is to identify and, if needed, approximate, the area of the domain that we define as the transition zone, that is where the flow from laminar becomes turbulent.

To this end, the friction velocity u_τ has been analysed. It is defined, in every point of the domain, as

$$u_\tau = \sqrt{\frac{\tau_w}{\rho}} = \sqrt{\nu \left.\frac{\partial u_m}{\partial y}\right|_{y=0}}$$

where τ_w is the local shear stress at the wall and it is given by the formula $(\rho\nu \, \partial u_m/\partial y)_{y=0}$, ρ is the fluid density and ν is the kinematic viscosity [12].

u_τ is used to normalise the coordinates and the velocities and allows us to identify the starting and ending points of the transition, considering its minimum and maximum values, respectively. These points are then located at $x/L = 204.3759$ and $x/L = 447.7873$, as it can be seen in fugure 4.1, and delimit an area before and after which the flow can be considered either laminar or completely turbulent.

4.2 Definition of the domain

In order to lighten the computational cost of the analyses, it has been chosen to reduce the domain to a smaller one, which remains nonetheless capable to depict

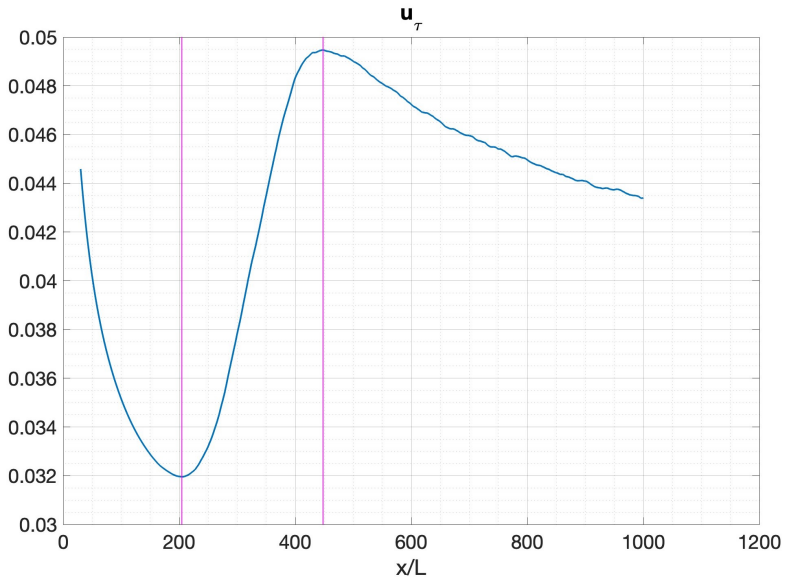

Figure 4.1: Local friction velocity u_τ. Lines in magenta outline the transition zone.

the variations and the complexities of the transitional boundary layer in all their shades.

This reduction has been made by sampling only some points of the datasets and, in particular, $N_x \times N_y \times N_z = 100 \times 72 \times 32$ points for three new intervals of the coordinates:

$$x/L \in [30.2185, 608.7952],\ y/L \in [0.0036, 6.1712],\ z/L \in [0, 232.6236].$$

The portions of the domain that have been excluded correspond, then, to a turbulent boundary layer, which we already know how it is supposed to function in terms of irreversibility [20], and to values of y/L sufficiently far from the wall, allowing us to focus only on what happens in the proximity of the wall and in the creation of the boundary layer.

In this new domain, the starting and ending point of the transition zone can be approximated to the closest point available, as it is summarised in the following table 4.1. The corresponding normalised values of x, $x^+ = xu_\tau/\nu$ are also specified.

4.3 Metrics and statistics

Before proceeding with the analysis of time irreversibility, it can be useful to observe what happens in the boundary layer in terms of mean velocities and turbulent

	value	approx. value	normalised value	approx. and norm. value
x_{start}	204.3759L	205.5448L	5.22466e+03	5.25469e+03
x_{end}	447.7873L	445.1573L	1.772373e+04	1.76141e+04

Table 4.1: Starting and ending points of the transition zone.

fluctuations, not only to have a complete picture of the system under study, but also to undertake a full disclosure on how the turbulence may be related to irreversibility.

4.3.1 Average velocities

A first analysis is performed on the streamwise component of the velocity u, by considering its time average at all the points of the domain. In figure 4.2 mean normalised velocities $u_m^+ = u_m/u_\tau$ are depicted on the $x^+ - y^+$ plane, where $x^+ = xu_\tau/\nu$ and $y^+ = yu_\tau/\nu$, after averaging over the 32 values of z.

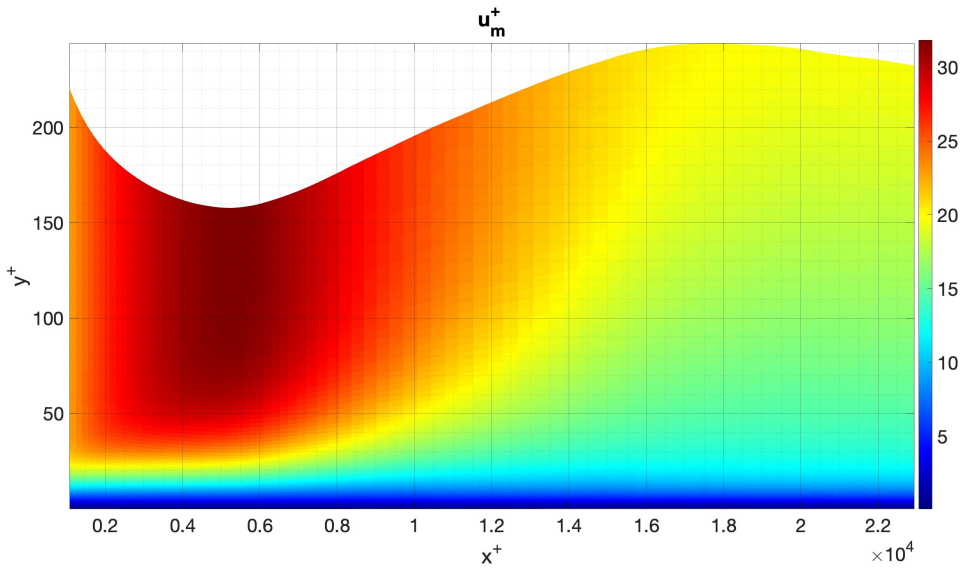

Figure 4.2: Normalised mean u velocities, averaged on z, on the $x^+ - y^+$ plane.

For small values of x^+ high values of u_m^+ are soon achieved, corresponding to those of the laminar flow. Conversely, increasing x^+, such values of u are reached more slowly and at higher values of y^+ (it should be noted that the new domain is limited on its upper part, hence high velocity values are not visible in this figure): this is representative of the growth of the boundary layer thickness. Normalising the coordinates allows us to observe how the boundary layer thickens with the onset

of transition, with a significant increase in the core area due to the turbulence development.

4.3.2 Fluctuations

u component

Turbulent fluctuations are defined by the Reynolds decomposition [12]:

$$u' = u - u_m$$
$$v' = v - v_m$$
$$w' = w - w_m.$$

Taking the root mean square of the velocity, it is possible to get a measure their intensity:

$$u_{rms} = \sqrt{\frac{1}{N}\sum_{i=1}^{N}(u_i - u_m)^2}$$

For the streamwise component, the average value on z of u^+_{rms} amplifies at the beginning and in the middle of the transition zone, along the boundary layer (figure 4.3). As x^+ increases, the intensity of the fluctuations decreases and is limited to an area quite close to the wall, while the peak moves towards it, just above a region of very low values. Downstream of the transition zone, fluctuations vanish more slowly and the distribution of a fully turbulent boundary layer is recovered.

Figure 4.4 shows how the peaks value vary with x^+ and how their maximum values correspond to the transition zone, indeed; the curve is increasing until the maximum in the zone, then it diminishes with almost stable values over a smaller range once the turbulence has fully developed, as noted above. Such peaks are located at increasing values of y^+, then, as the transition begins, they approach the wall and stabilise around a certain value in the fully turbulent flow, as can be noted in figure 4.5.

v and w components

Instead, turbulent fluctuations of the wall-normal (figure 4.6) and spanwise (figure 4.7) components develop exactly in the transition zone, being finite but almost null upstream of the leading edge, then gradually increase until reaching the fully turbulent state. As in the previous case, as y^+ grows, fluctuations tend to zero

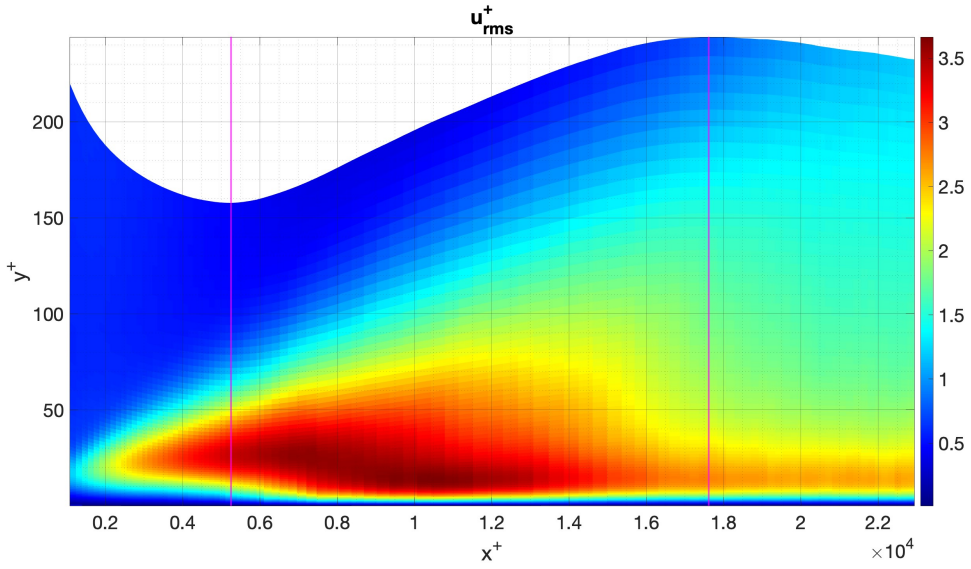

Figure 4.3: Intensity of the turbulent fluctuations of the u component of the velocity, averaged on z, on the $x^+ - y^+$ plane. Lines in magenta outline the transition zone.

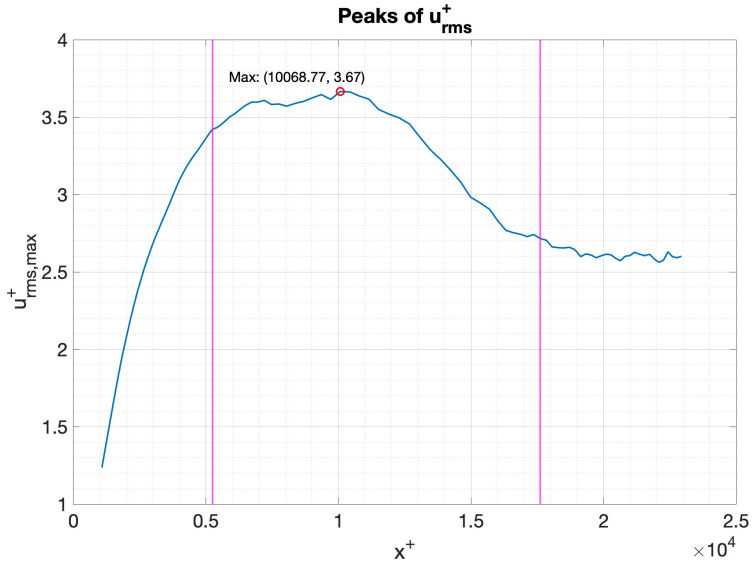

Figure 4.4: Maximum values of u^+_{rms} with respect to x^+. The maximum of these peaks is highlighted in red. Lines in magenta outline the transition zone.

when exiting the boundary layer. However, for these components, the range of y^+ that is affected by more intense fluctuations is broader. At the leading edge, slight fluctuations are caused by the isotropic turbulence impacting the plate. This is also

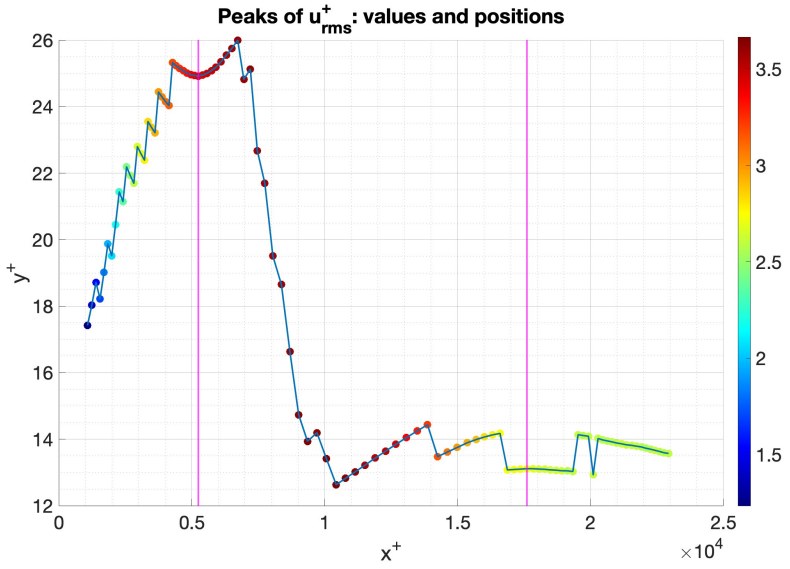

Figure 4.5: Values of the maxima of u^+_{rms} and their positions on the $x^+ - y^+$ plane. Lines in magenta outline the transition zone.

visible in the analysis of their peaks, with a small maximum fluctuation decreasing in the laminar flow zone (figures 4.8). The trend of the peaks then grows rapidly, marking the transition zone, and, towards the end of this, tends to stabilise at an approximately constant value. This trend is the same found for the friction velocity u_τ.

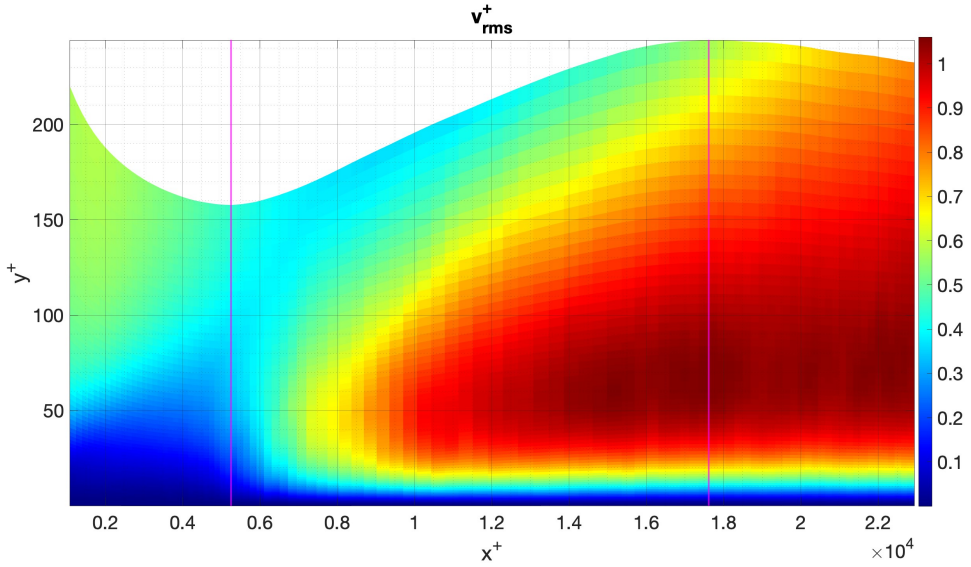

Figure 4.6: Intensity of the turbulent fluctuations of the v component of the velocity, averaged on z, on the $x^+ - y^+$ plane. Lines in magenta outline the transition zone.

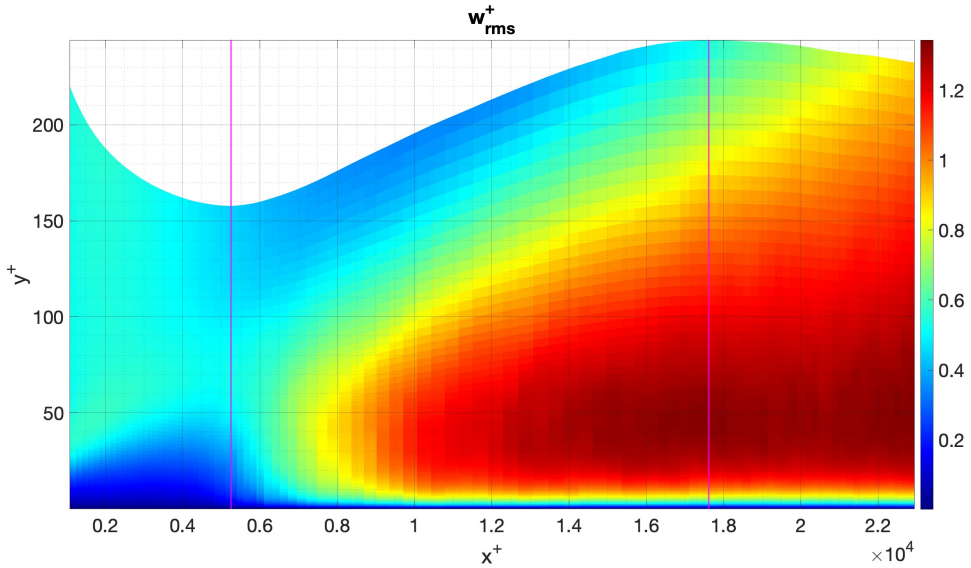

Figure 4.7: Intensity of the turbulent fluctuations of the w component of the velocity, averaged on z, on the $x^+ - y^+$ plane. Lines in magenta outline the transition zone.

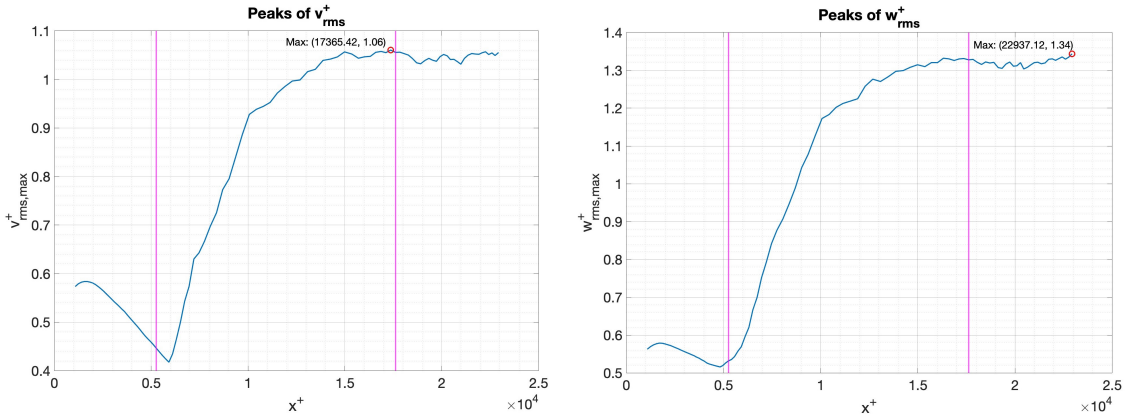

Figure 4.8: Maximum values of v^+_{rms} (left) and w^+_{rms} (right) with respect to x^+. The maximum of these peaks is highlighted in red. Lines in magenta outline the transition zone.

Chapter 5

Results

5.1 Irreversibility measure

Finally, the aim of this study is to calculate the time irreversibility of a transitional boundary layer. It has to be noted that the case of transition is known to be statistically non-stationary - differently from fully developed turbulence - and, by definition, non-stationary time series are infinitely irreversible. Hence, it is already known that the signals are irreversible, but the application of the visibility method stands to quantify how much the signals are irreversible, that is, the degree of irreversibility.

As it has been seen in paragraph 3.3.3, a reliable measure of time irreversibility is represented by the Kullback-Leibler divergence (KLD) of the ingoing degree k_{in} and outgoing degree k_{out} probability distributions of the nodes of the visibility graph:

$$I_k = \sum_k P_{out}(k)\ log\frac{P_{out}(k)}{P_{in}(k)}.$$

The KLD, here defined by the notation I_k, is null in case of reversible signals, and it assumes growing values in the presence of strong levels of irreversibility (even though it is important to recall that it is exactly zero only in the ideal case of infinitely long signals).

In the following, time irreversibility will be first localised spatially within the 3D domain and then it will possibly be linked to the turbulent structures that characterise the transitional boundary layer.

u component

In the case of z fixed (figure 5.1), small areas with higher values, ranging from 0.2 to 0.5, are scattered at different points in the $x-y$ plane, starting near the beginning of the transition zone and moving towards the centre. This may be attributed to the presence of isolated turbulent spots distributed in the boundary layer that will slowly evolve and burst into turbulence once downstream of the zone.

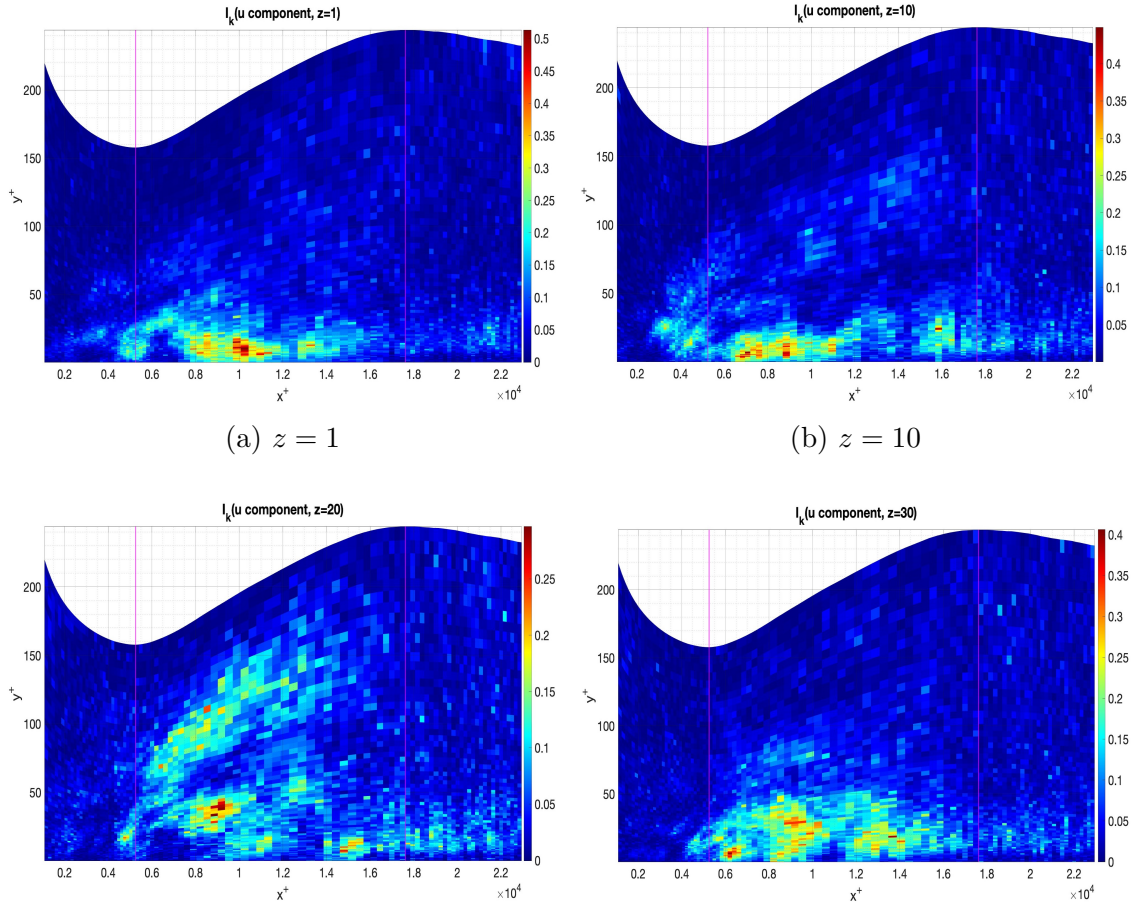

(a) $z = 1$ (b) $z = 10$

(c) $z = 20$ (d) $z = 30$

Figure 5.1: Irreversibility I_k calculated for the u component of the velocity at 4 fixed values of the coordinate z on the $x^+ - y^+$ plane. Lines in magenta outline the transition zone.

Averaging on z (figure 5.2) enables the visualisation and identification of a relatively expanded area of high irreversibility, with values in the range $0.1 - 0.2$, located at the centre of the transition zone and very close to the wall, which then

gradually fades increasing y^+. In the downstream region of the transition zone, a tail-shaped area of irreversibility is observed, but with a medium intensity around 0.1. This area is confined to a limited range of y^+ values, situated just above the wall and its position is analogous to that identified in the turbulent fluctuations analysis depicted in figure 4.3. It has to be noted that a lower intensity irreversibility zone, with values just below 0.1, is already attained before the starting point of the transition: this could be due to the averaging of the initial turbulent streaks that originate exactly in this area [13].

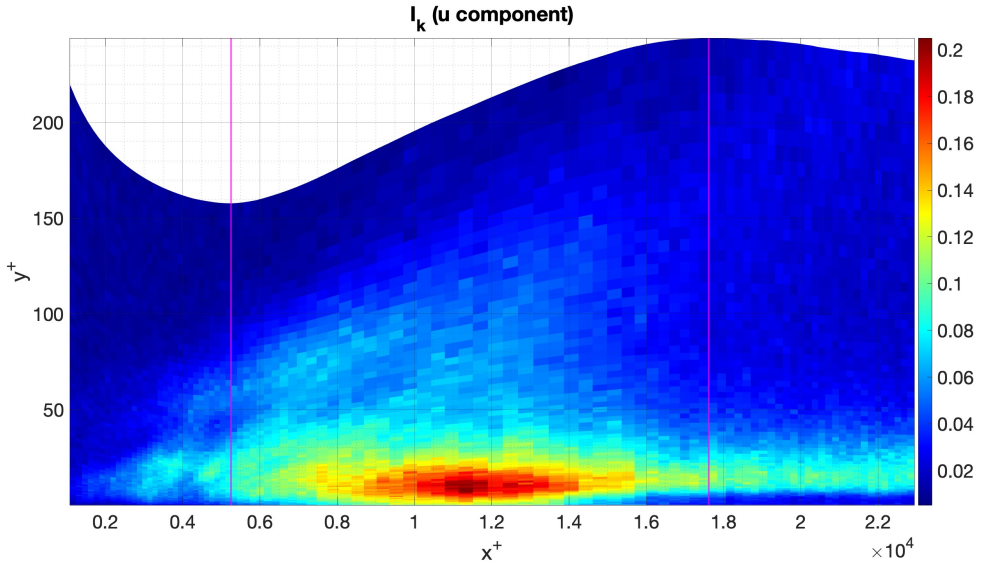

Figure 5.2: Irreversibility I_k average value on z calculated of the u component of the velocity on the $x^+ - y^+$ plane. Lines in magenta outline the transition zone.

v and w components

For the wall normal and spanwise components, whose behaviour is shown directly after the averaging on z in figures 5.3 and 5.4, the values of I_k are around one order of magnitude lower, but coherently with the characterisation of these components. Also in these cases, it is possible to define a well-delimited area of irreversibility with values between 0.02 and 0.05. It is located close to the wall and it already begins across the start line of the transition zone spreading until its center, and vanishing for higher y^+s. Very low values of the order of 0.02 are also retrieved in the fully turbulent flow area in the proximity of the wall. Here we cannot establish a direct correspondence with the position of turbulent fluctuations, which suggests

that the matter of what causes irreversibility is not trivial and requires further investigation.

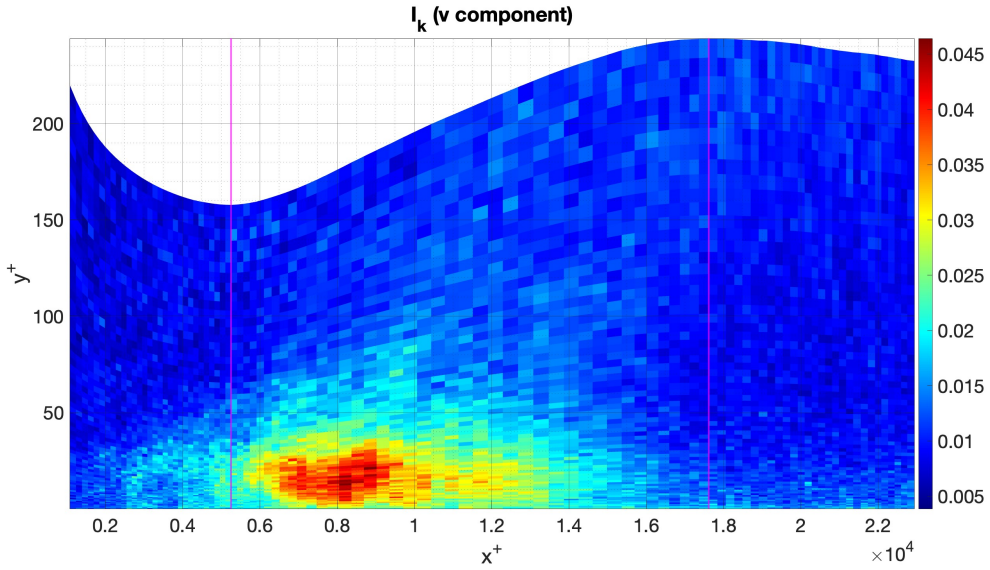

Figure 5.3: I_k average value on z calculated of the v component of the velocity on the $x^+ - y^+$ plane. Lines in magenta outline the transition zone.

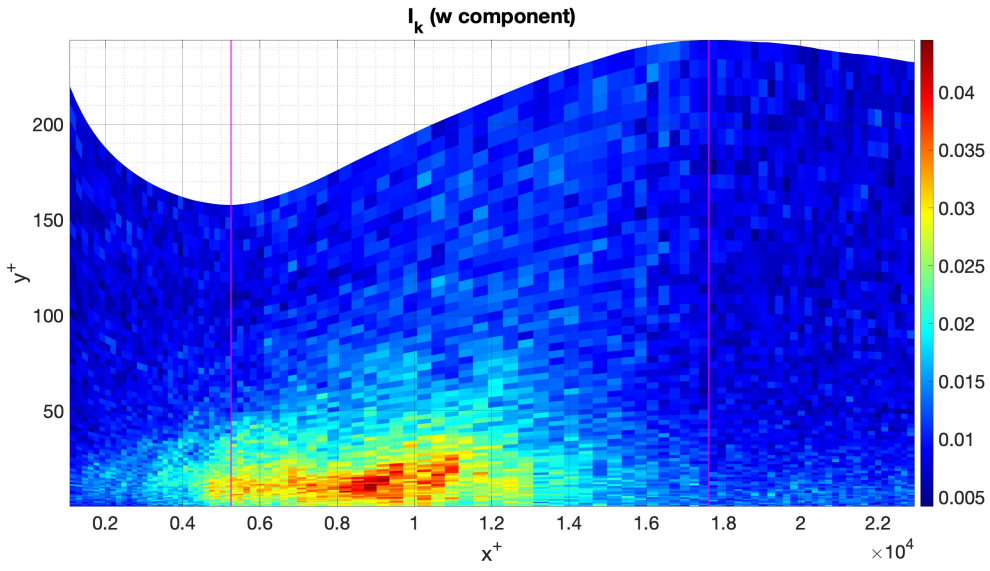

Figure 5.4: I_k average value on z calculated of the w component of the velocity on the $x^+ - y^+$ plane. Lines in magenta outline the transition zone.

5.1.1 Reliability of the method (Z score)

While it has been seen that positive values of I_k are easily recovered, it is important to verify that such positive values are actually reliable in quantifying time irreversibility. To do so, as it has been already done in previous studies [20, 51], and as it has been pointed out in paragraph 3.3.4, the Z-Score of I_k can be calculated as

$$I_{k,r} = \frac{I_k - \mu_{k,r}}{\sigma_{k,r}}$$

High values of this measure can be considered as a confirmation of time irreversibility. Here $\mu_{k,r}$ and $\sigma_{k,r}$ represent respectively the mean and the standard deviation of I_k calculated on an ensemble of random signals, which have been obtained from the original time-series signals by shuffling the 4701 time steps.

A first attempt has been made by computing 20 permutations of the time series' time step and by observing all the $x-y$ planes at different z values, concentrating, for now, only on the u component of the velocity. A problem that has been soon detected is the presence of some negative values of $I_{k,r}$, whose meaning is to be attributed to irreversibility values lower than the mean of the random signals, which by definition should be reversible.

Actually, already in the calculation of I_k, the 0.0001% of the values resulted negative: this has no meaning being I_k a KLD, which by definition assumes only non-negative values. However, this phenomenon can be explained by observing that the time series analysed are quite short and do not contain enough points to confer robustness to the calculation. After having ensured that this was related neither to a mistake in the code nor to a flaw in the randomisation process for the calculation of the permutations, the problem has been circumvented by ignoring these points. Nevertheless, $I_{k,r}$ still exhibits around 10% of its values as negative, the explanation for which remains linked to the length of the time series.

To visually show this, let's see the case of 20 permutations of the time steps of the time series at $z = 1$, in figure 5.5. All $I_{k,r}$s with a value below 2 are highlighted, as they are very low (hence, not very reliable) or even negative: they are prevalently localised outside the transition zone and very close to the wall or outside the boundary layer (a representation of the $x-y$ plane with respect to the normalised coordinate y/δ, where δ is the boundary layer thickness, has been

chosen to point out this feature.)

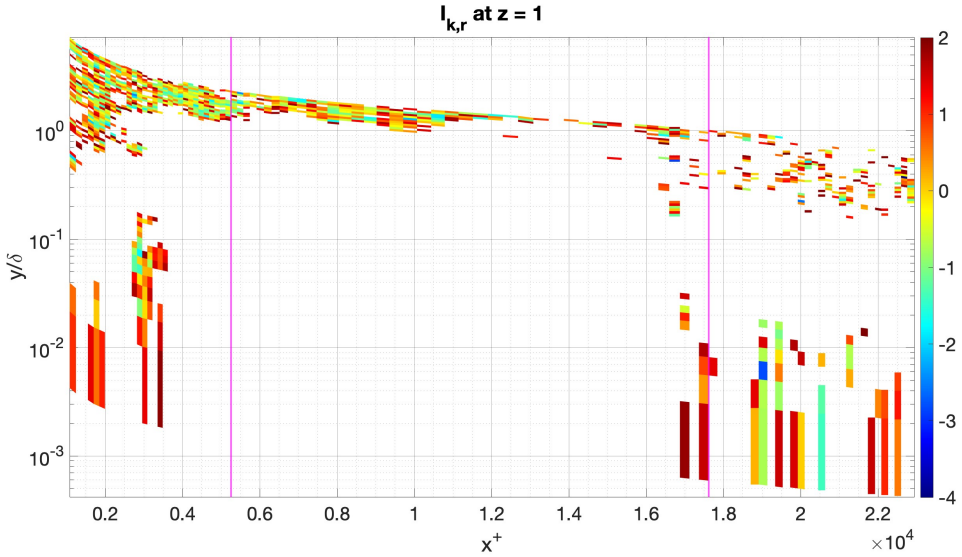

Figure 5.5: Irreversibility ratio $I_{k,r}$ evaluated at $z = 1$, considering its lowest values on the $x^+ - y^+$ plane, having chosen $I_{k,r} = 2$ as threshold. Lines in magenta outline the transition zone.

Consequently, a small investigation has been performed on a few points x of the domain, where significant variations of $I_{k,r}$ were present, from high to very low values, such as those indicated by the black lines in figure 5.6. Figure 5.6 represents in full the values of $I_{k,r}$, considering all values above 10 as "high".

As an example, here the analysis on the point $x = 73$ (which correspond to $x/L = 451.0016$ and $x^+ = 17842$) is reported for some values of y: $y = 12$ ($y/\delta = 0.033$), $y = 39$ ($y/\delta = 0.219$), $y = 44$ ($y/\delta = 0.282$), $y = 58$ ($y/\delta = 0.546$). Figure 5.7 depicts the behaviours of $I_{k,perm}$, the irreversibility measure calculated after permuting the points of the time series, as the permutations were performed. Their mean values ($\mu_{k,r}$) and their standard deviations ($\sigma_{k,r}$) are also shown. The clear oscillatory character is again a symptom of a too short signal length and is present at all points analysed, even when performing a greater number of permutations.

The final step entailed increasing the number of permutations to 30, then 40, then 50 and in some cases 100, with a view to ascertaining whether this parameter could make the calculation more robust. This is indeed true, as an augmentation in the number of permutations engenders, in a certain sense, a greater degree of randomness in the signal in comparison to the original one, and allows a more

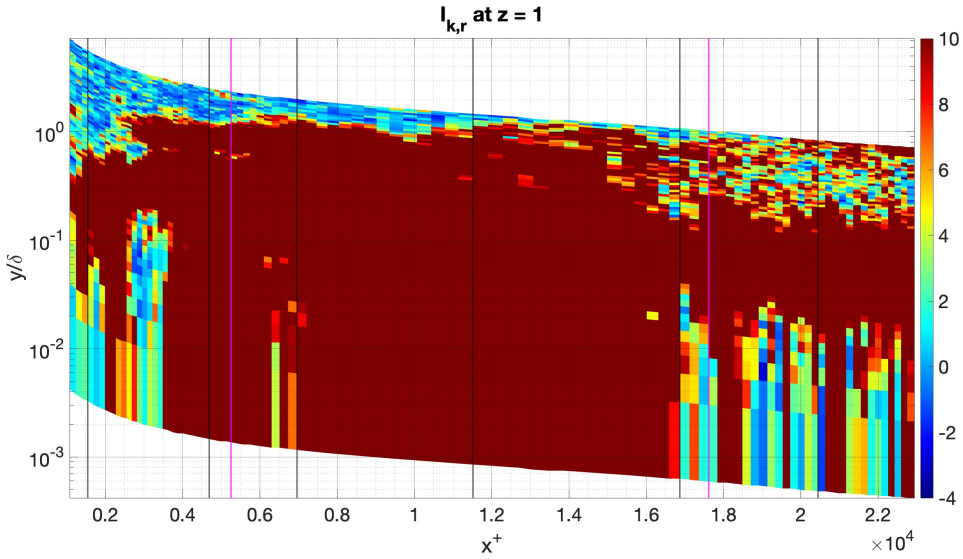

Figure 5.6: Irreversibility ratio $I_{k,r}$ evaluated at $z = 1$, highlighting its highest values on the $x^+ - y^+$ plane, having chosen $I_{k,r} = 2$ as threshold. Lines in magenta outline the transition zone.

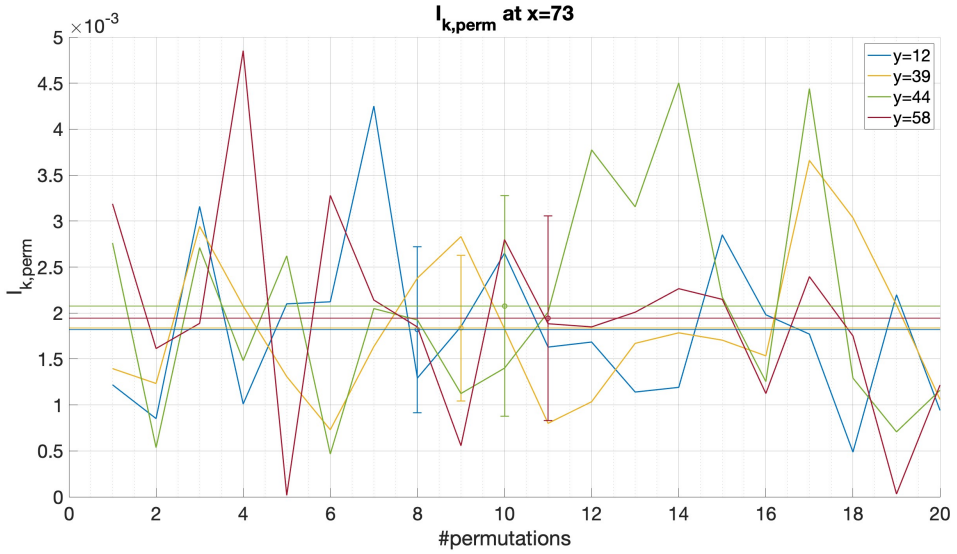

Figure 5.7: How the irreversibility measure at $x = 73$ changes while increasing the number of permutations of the time series' points. Each color represent a different y value at the same x coordinate.

reliable comparison.

For 50 permutations, behaviours analogous to those illustrated in figure 5.6 have

been identified in each z-plane. In order to obtain a more valid statistical evaluation, the results have been averaged on z, thereby eliminating the "critical" points, i.e. those that are too low or negative, and making the distribution of the $I_{k,r}$ values more uniform. This verifies that, from a statistical perspective, the calculation is both valid and reliable, as illustrated in figure 5.8. In fact, at the centre of the transition zone, where major irreversibility was supposed to be found, $I_{k,r}$ reaches values of the order of 10^2 and values slightly below in the surrounding area.

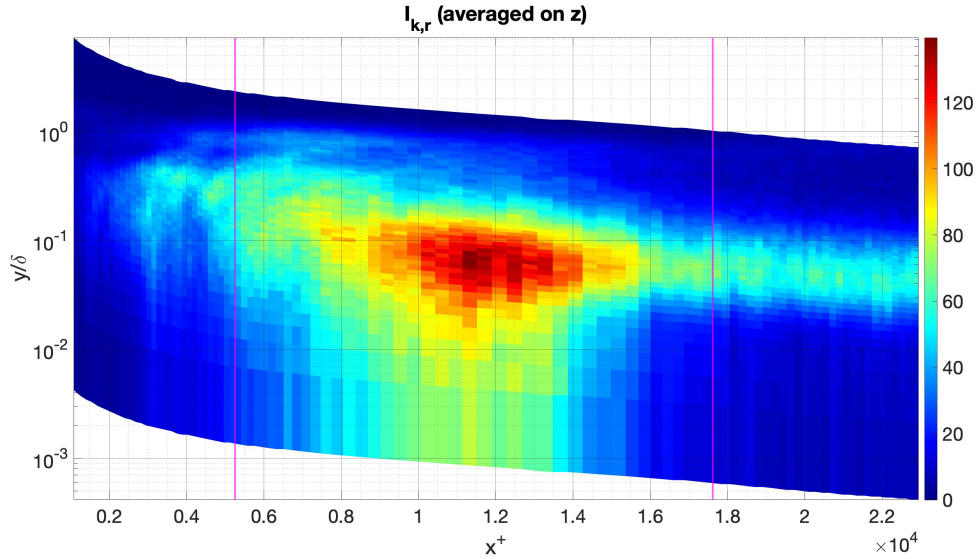

Figure 5.8: Irreversibility ratio $I_{k,r}$ average value on z, on the $x^+ - y/\delta$ plane. Lines in magenta outline the transition zone.

Finally, for comparison, the behaviour of I_k is also reported in figure 5.9 and it appears identical to the one of $I_{k,r}$. This is due to the fact that averages and standard deviations (figure 5.10) do not show any pattern on the $x - y$ plane, allowing $I_{k,r}$ to retain the original pattern of I_k. It is confirmed, therefore, the presence of a zone with high irreversibility in the center of the transition zone, followed by a "tail" in the totally turbulent zone.

Localisation of irreversibility within the $x-y$ plane of the boundary layer

The turbulent fluctuations and $I_{k,r}$ are again displayed, this time with a logarithmic scale for the y-axis representing y^+, in order to discuss their correlation in terms of the boundary layer structure.

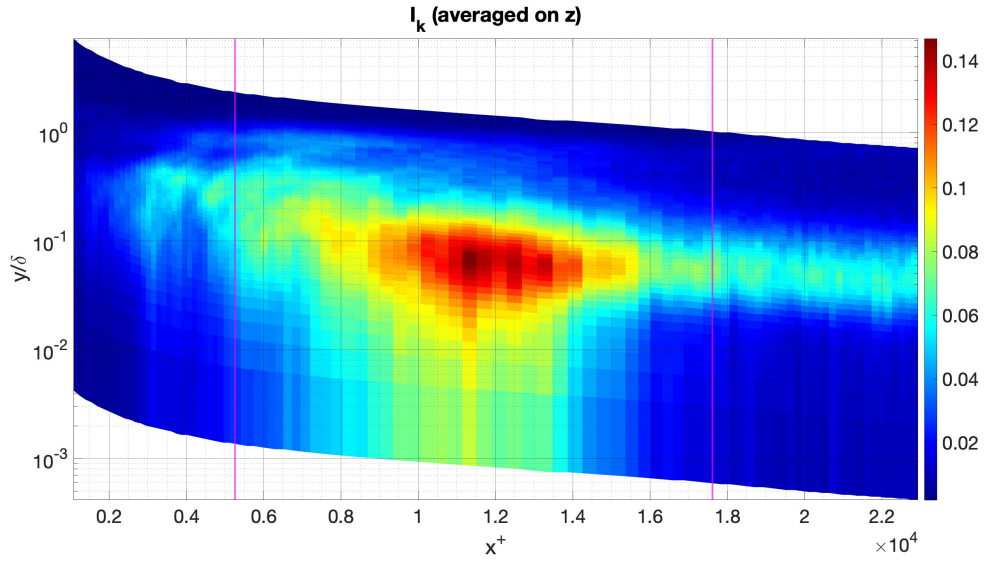

Figure 5.9: Irreversibility I_k average value on z, on the $x^+ - y/\delta$ plane. Lines in magenta outline the transition zone.

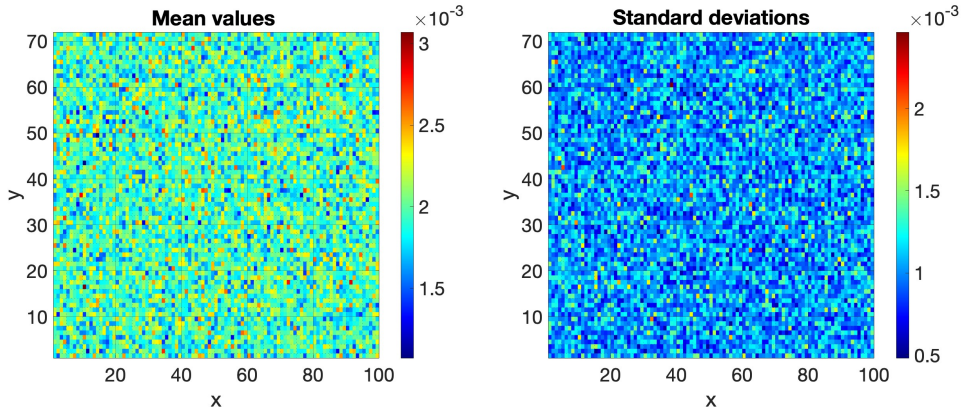

Figure 5.10: $\mu_{k,r}$ and $\sigma_{k,r}$ mean and standard deviations of $I_{k,perm}$ on the $x - y$ plane.

It is recalled that the boundary layer can be parted into different wall regions and layers, depending on the value of y^+, with different defining properties [12]:

- viscous sublayer ($y^+ < 5$)
- buffer layer ($5 < y^+ < 30$)
- viscous wall region ($y^+ < 50$)
- log-law region ($y^+ > 30$)

- inner layer ($y^+ < 10^3$)
- outer layer ($y^+ > 50$)
- overlap region between inner and outer layer

It is known that the maximum turbulent activity in terms of production of kinetic energy is to be located in the buffer layer. This phenomenon can be graphically seen in figure 5.11, where turbulent fluctuations reach their highest levels exactly in the buffer layer.

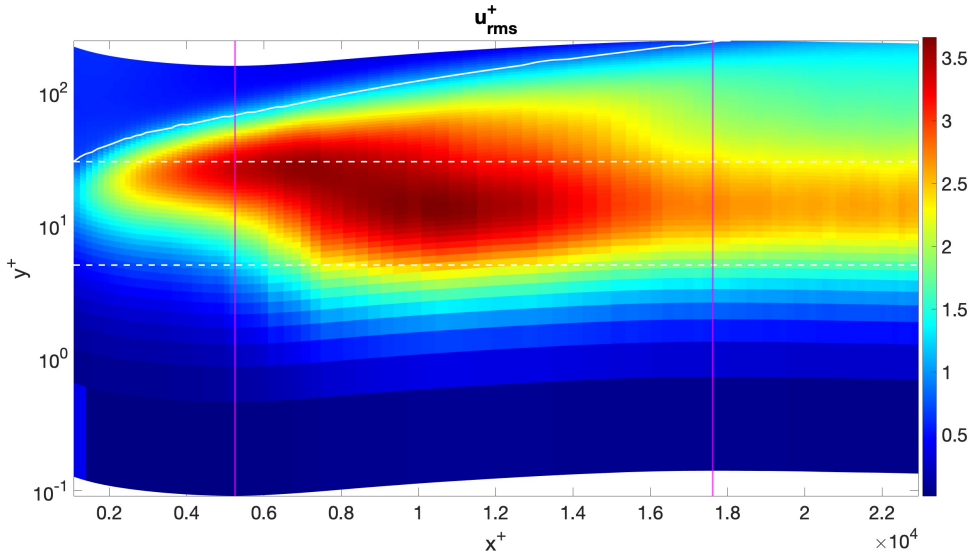

Figure 5.11: Intensity of the turbulent fluctuations averaged on z on the $x^+ - y^+$ plane. The white dashed lines delimit the buffer layer and lines in magenta outline the transition zone.

In figure 5.12 it can be seen how also in the case of $I_{k,r}$ highest values are achieved in the buffer layer and in particular in the transition zone, but also in the fully turbulent flow area. In the viscous sublayer the irreversibility remains high at the transition zone, while both before and after it there are almost zero values, as already noted above.

5.2 Local analysis by windows

Once the time irreversibility has been located spatially in the domain, its causes need to be investigated. The question pertains to the potential association of the

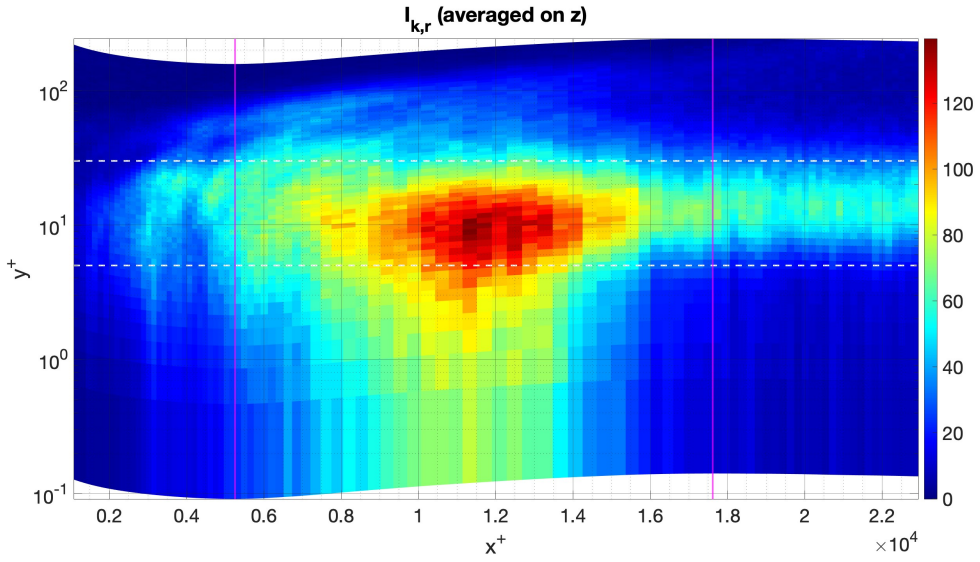

Figure 5.12: Irreversibility ratio $I_{k,r}$ average value on z, on the $x^+ - y^+$ plane. The white dashed lines delimit the buffer layer and lines in magenta outline the transition zone.

phenomenon with any structure that constitutes the transitional boundary layer.

Literature clearly portrays the transitional boundary layer structure and the bypass transition, [13, 14, 28, 33, 34] where the boundary layer transitions from laminar to turbulent flow bypassing some events that are typical of a normal laminar–turbulent transition. The evolution of the flow is characterised by a first shear sheltering phase, that allows the penetration in the boundary layer of low frequency components only, sheltering high frequency ones; then these perturbations are distorted into streaks, turbulent structures elongated in the streamwise direction, whose amplitude can reach over 10% of mean velocities. At a critical value, thanks to secondary instabilities, they randomly burst into turbulent spots, that grow all over the boundary layer and congregate forming the fully turbulent region.

The observation of the time series in paragraph 3.2 had already highlighted the great intermittency characterisation of the signals belonging to the transition zone. These signals are marked by turbulent spots, which increase in intensity and size with the increase of the x and y coordinates and which are arranged variably with

the variation of the z coordinates. The preliminary idea is that higher fluctuations and intermittency are associated to higher irreversibility. To verify such hypothesis it is necessary to identify and locate the turbulent spots in order to link them to a certain I_k value.

The procedure that has been chosen to investigate such aspects is a local analysis of I_k by window, that is using moving temporal windows on the time series' signals. This allows isolating bit by bit pieces of the signal that have different types of intermittency and being able to compare them with the whole signal.

The signal should be divided into 500-point windows with a 50% overlap, on each of which irreversibility I_k is to be calculated. Subsequently, 20 random signals should be generated for each window by permuting the time series points, allowing for the computation of the irreversibility ratio $I_{k,r}$. Instant turbulent fluctuations of the velocity $u' = u - u_m$ are also required in order to research a potential correlation with irreversibility.

Before an overall analysis of the whole domain, a focused investigation has been conducted on a specific z coordinate (in this case, $z = 1$ has been chosen) and a few x and y points, with the objective of elucidating the occurrences in that particular area.

The choice of points was made considering the point (x, y) in which $I_{k,r}$ assumed maximum value and exploring, at that same x, some y that presented quite different values of $I_{k,r}$ on the complete signal.

As shown in figure 5.13, the oscillatory behaviour of $I_{k,r}$ on windows does not correspond to turbulent fluctuations (mediated on the same window). Conversely, there are instances where high values of u_{rms} are concomitant with low values of $I_{k,r}$.

Even with increasing the number of permutations used to generate random signals, the trends in $I_{k,r}$ remain relatively similar, but with a slight improvement, as illustrated in figure 5.14.

In order to investigate the oscillatory behaviour, the time windows have been observed directly in a view similar to that shown in figure 5.15. This observation has led to the hypothesis that the increase in the values of $I_{k,r}$ is linked to zones which could be designated as "overlap", that is, those pieces of signal in which it

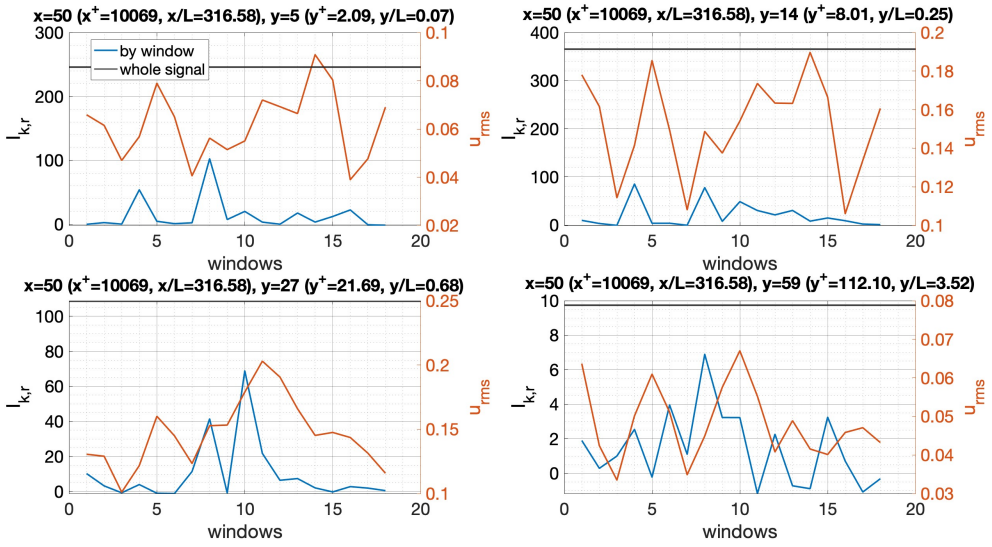

Figure 5.13: Irreversibility ratio $I_{k,r}$ calculated by windows and for the whole signal, compared to turbulent fluctuations in four points of the domain at the same x-coordinate.

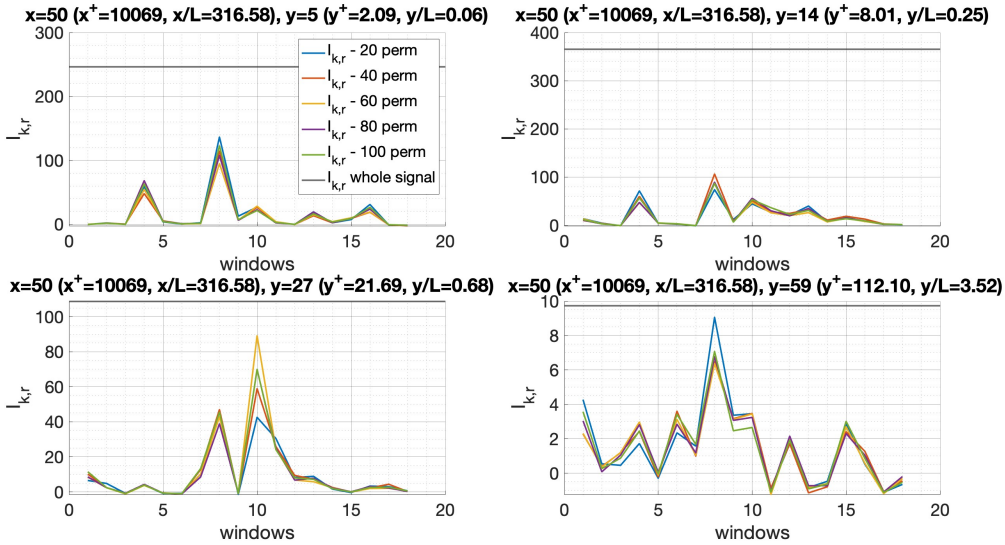

Figure 5.14: Irreversibility ratio $I_{k,r}$ calculated by windows increasing the number of permutations and for the whole signal in four points of the domain at the same x-coordinate.

passes from being very fluctuating to being flat, rather than to areas with many

fluctuations. The explanation would be that in such cases the signal is very asymmetric and the visibility method is designed to capture the geometry of the signal rather than its amplitude. Consequently, signals characterised by significant fluctuations yet greater geometrical uniformity may, nevertheless, yield lower values.

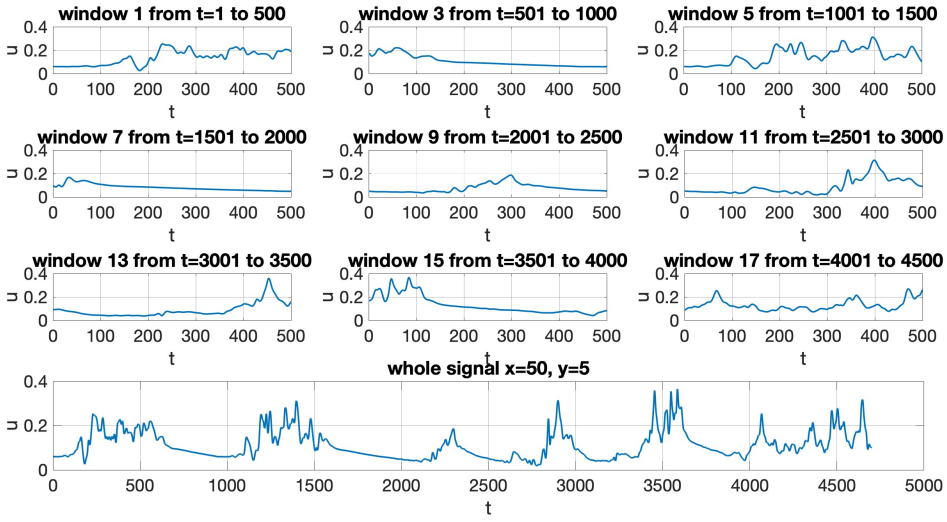

Figure 5.15: Visualisation of the moving windows every 500 points - without considering the overlap - on a time series and the whole signal.

5.2.1 Analysis of an intermittent signal

The subsequent stage of the process has been to manually search the transition zone for an intermittent signal in which there were one or two turbulent spots that were well-defined in comparison to the rest, then to manually define the time length of the spots to be used as a moving window, in order to understand what happens before, during, and after the spot in the signal.

This has been done as in figure 5.16, where the areas of the spots and those preceding and succeeding them are highlighted. For the sake of convenience, the latter ones are referred to as 'laminar' in the subsequent figures. The overlap windows between these are designated 'in' and 'out', as if one were 'entering' and 'exiting' the spot.

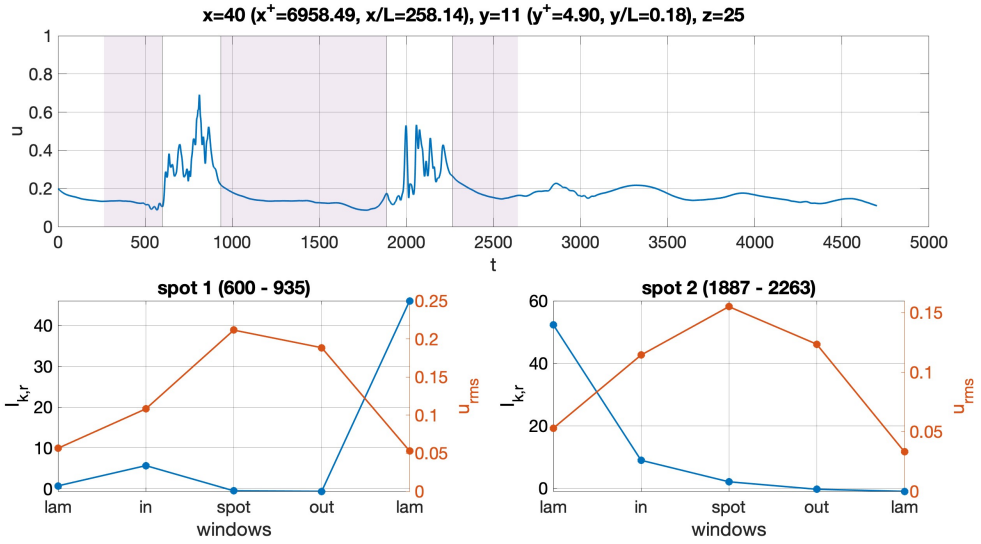

Figure 5.16: Analysis by customised windows on a signal. Above the windows are identified on the signal, highlighting in violet the 'laminar' windows preceeding and succeeding the spot. Below the values of $I_{k,r}$ for the five windows of the two spots.

The peculiarity of these results is that once again the highest values of $I_{k,r}$ do not correspond to the windows that include the spots; rather, a higher value is observed "entering" the spot, or even in the laminar zone between the two spots. It is important to note that the visibility method is significantly influenced by the length of the signal under analysis, as pointed out in paragraph 3.3.4, and in this particular instance the signal is very short. Furthermore, the method is based primarily on symmetry and geometric criteria rather than amplitude ones.

Comparison between the Kullback-Leibler divergence and the Jensen-Shannon divergence

To explore the full range of possibilities and drawing inspiration from other studies [52], the analysis has been extended to include the Jensen–Shannon divergence, a more robust and symmetric measure compared to the Kullback–Leibler divergence previously adopted. It is defined as

$$JSD(P||Q) = \frac{1}{2}D(P||M) + \frac{1}{2}D(Q||M),$$

where P and Q are probability distributions, $M = \frac{1}{2}(P + Q)$ is a distribution's average and $D(\cdot||\cdot)$ is the Kullback-Leibler divergence. As can be seen in figure

5.17, the discrepancy is negligible; therefore, it has been opted to persist with the Kullback-Leibler approach while concurrently maintaining this alternative as a possibility.

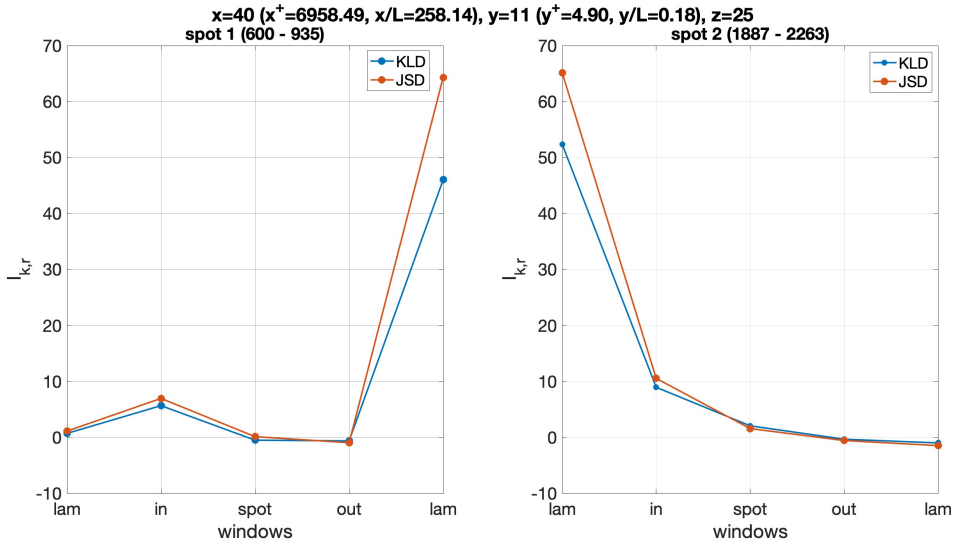

Figure 5.17: Comparison between the $I_{k,r}$ values calculated with the Kullback-Leibler divergence - in blue - and the Jensen-Shannon divergence - in orange - on five windows for each spot.

5.2.2 Analysis on the turbulent fluctuations

The analysis continues by considering several windows on the same signal. The primary issue with this form of observation is that even the regions designated as "laminar" exhibit minor fluctuations, which, as previously mentioned, are detected by the visibility graph method. Furthermore, the manual selection of windows does not follow a rigorous and precise criterion for identifying the point of origin and end of a specific spot and does not allow an easy generalisation on all signals.

The methodological problem of spot detection becomes then an issue, but research in the literature indicates that, in the case of boundary layers subjected to the effect of an undisturbed flow turbulence, the use of the u component of speed is not effective for spot detection; instead, components v and w may be. [53]

It is evident from figure 5.18, representing the turbulent fluctuations' signals, that the visibility of spots is intensified. However, it is important to note that

a more reliable identification can be achieved through the implementation of a thresholding technique on the values of v and w.

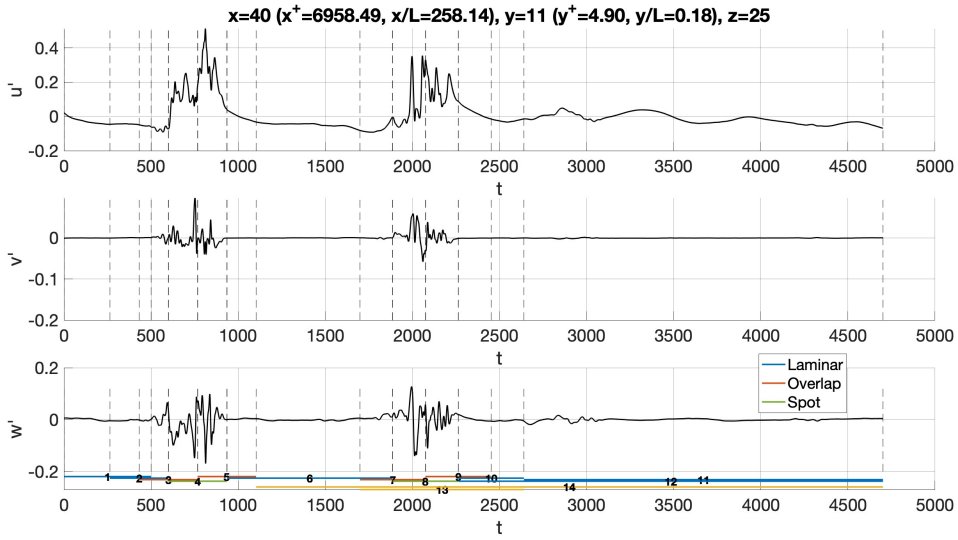

Figure 5.18: Time series of the fluctuations of the velocity. Different time windows are highlighted in different colours: in blue laminar parts of the signal, in orange the overlaps, in green the spots and in yellow mixed types of windows.

Analysing the turbulent fluctuations on all three components of the velocity, the previous procedure has been repeated by including, in addition to those of the spot, overlap and laminar, new windows that include both exclusively "laminar" zones - such as windows 10, 11, 12 - and windows that include laminar zones and spots together - such as 13 and 14 (figure 5.18).

This is to make a cumulative comparison, with the aim of understanding what happens to $I_{k,r}$ by adding and removing turbulent pieces to a "laminar" signal. The cumulative comparison is motivated by the fact that, according to the calculations made so far and due to the problem of signal length which affects the method, it may not make sense to take turbulent and laminar pieces separately.

However, according to figure 5.19, once again no well-defined patterns can be observed in the values of $I_{k,r}$. High values are present in the areas defined as "laminar" and in some cases in the overlap zones, and this is motivated, as already mentioned, by the geometric approach of visibility.

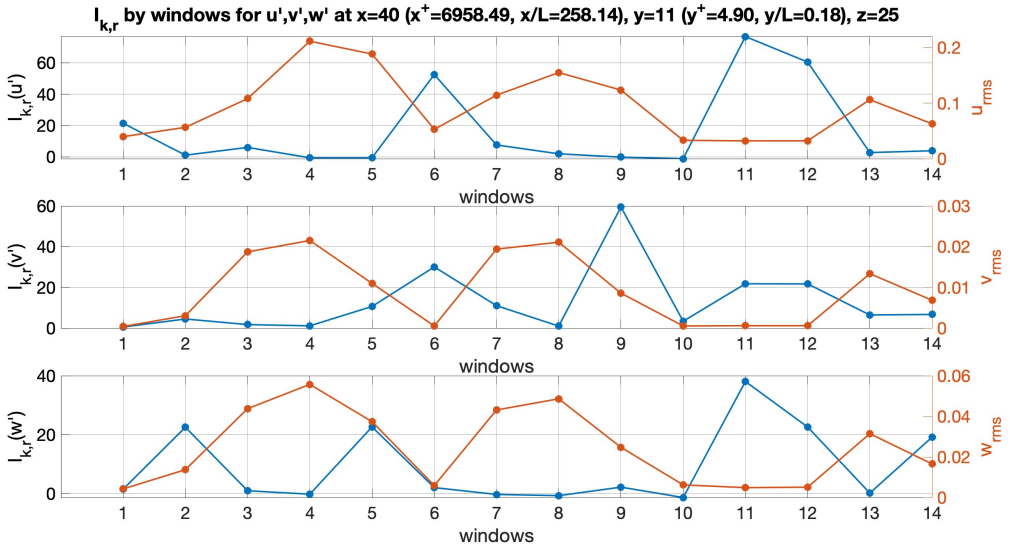

Figure 5.19: Irreversibility ratio $I_{k,r}$ calculated by windows of different length (depicted in fig. 5.18) and compared to turbulent fluctuations for the three components of the fluctuations.

5.2.3 Comparison between horizontal visibility graph and natural visibility graph

So far, the analysis carried out showed that the irreversibility measure $I_{k,r}$ is not directly related to turbulent fluctuations of the signal, but seems to be more affected by the transition zones between laminar and turbulent parts of the signal, therefore the analysis of these individual parts is less effective than a cumulative analysis of more signal pieces.

This is due to the fact that the visibility graph method captures more the geometric structure of the signal than its amplitude, leading to high irreversibility values even in regions that do not contain turbulent spots, but have significant variations in the signal morphology.

In an attempt to address the issue of signal length, the Natural Visibility Graph has also been implemented, in order to provide a more comprehensive overview of the results. In comparison to the Horizontal Visibility Graph, the Natural Visibility Graph has the capacity to establish a greater number of links, due to the fact that the visibility of a node on other nodes is not limited solely to the horizontal dimension, but extends to all locations that are intervisible.

An initial comparison has been conducted by considering the measures I_k and $I_{k,r}$ on all signals averaged on z. Figure 5.20 shows how higher levels of time irreversibility are achieved, with the use of the NVG, mainly in the first part of the transition zone. The highest values of both I_k and $I_{k,r}$ are confined to an area that includes the pre-transition zone, where turbulence starts to develop, and to points in the very proximity of the wall, differently with respect to HVG. In the case of NVG, the tail-shaped area retrieved with the HVG, is instead absent.

The NVG, thus, focuses irreversibility in a region corresponding to the most active one in terms of the turbulence development and is less related to the behaviour of the fluctuations, unlike the HVG.

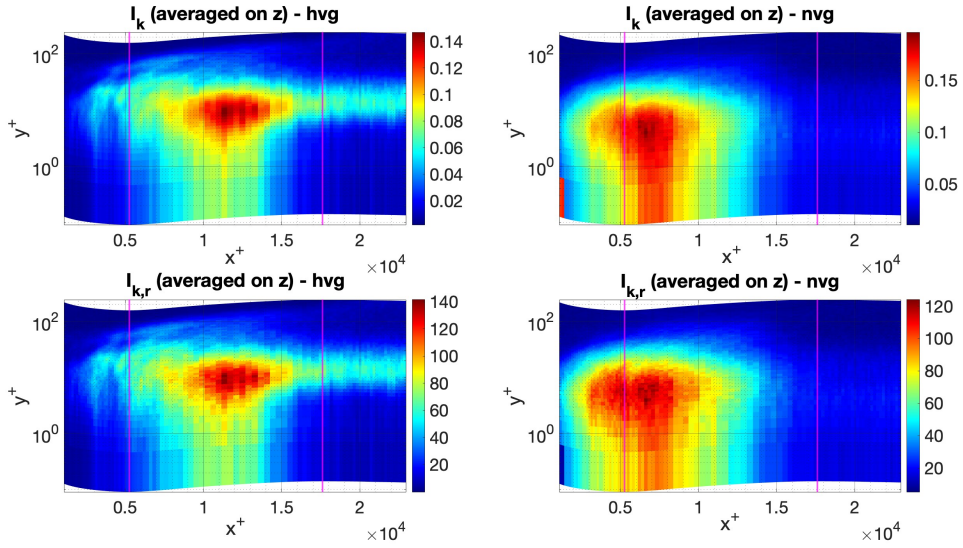

Figure 5.20: Comparison of values of I_k and $I_{k,r}$ when using HVG or NVG, on the $x^+ - y^+$ plane, averaging on z.

In the analysis by windows, in order to obtain a more detailed characterisation of the signals, the NVG method has been also applied in a modified version, here called Bottom-NVG (BNVG), which consists in applying the NVG to the signal after changing its sign. This procedure allows to highlight the connections between the local minima of the series - instead of the maxima, as the NVG does - and to observe the vertical symmetry of the signal, and consequently its global asymmetry when compared to the original one. It then provides additional and complementary information to those obtained with the classic NVG.

Fixed time window length

In the following analyses, longer and constant time windows have been used to overcome the issues previously mentioned.

Taking again as a reference the previously used signal 5.21, which is located within the transition zone and exhibits two discernible turbulent spots, the time windows that have been chosen have length equal to half of the signal (2350 time steps) and move forward in time by 235 time steps.

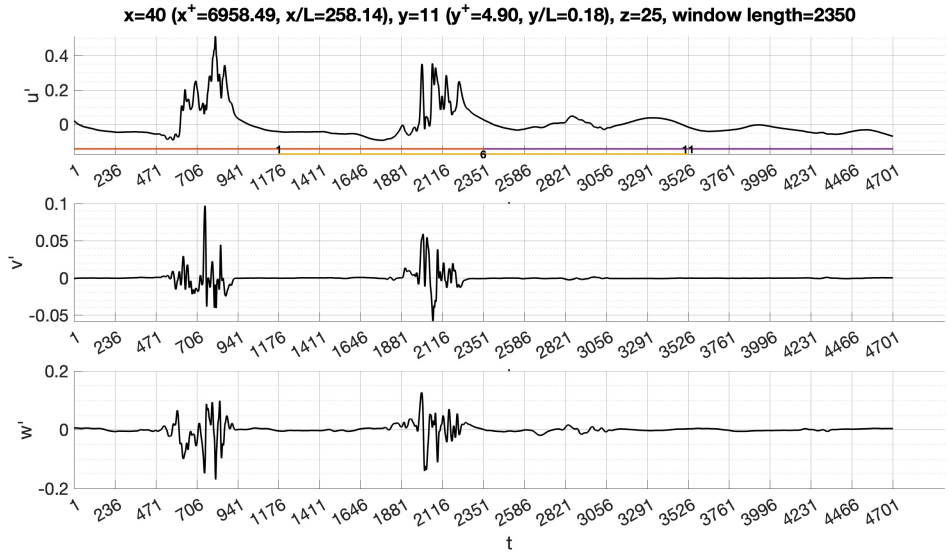

Figure 5.21: Time series of the fluctuations of the velocity. Windows' length is 2350 and they move every 235 time steps. Three different time windows are highlighted in different colours as an example of same-length windows.

The first observation, as illustrated in figure 5.22, is that, in general, both NVG and BNVG yield higher values of $I_{k,r}$ in comparison to HVG, either considering the signal as a whole or considering individual windows. Moreover, the use of sufficiently long windows and a high number of permutations (500) ensures a greater correlation between the trend of $I_{k,r}$ and the average fluctuations of the three components of the speed (u_{rms}, v_{rms}, w_{rms}) on the windows, particularly with the BNVG. However, it should be noted that this is not a one-to-one match.

Another interesting example is the signal in figure 5.23 which is also belonging to the transition zone and exhibit a single turbulent spot. In this case the time windows' length has been set to 1880 instants, thus enabling analysis of windows exhibiting solely laminar signals, as well as windows including the spot in part or

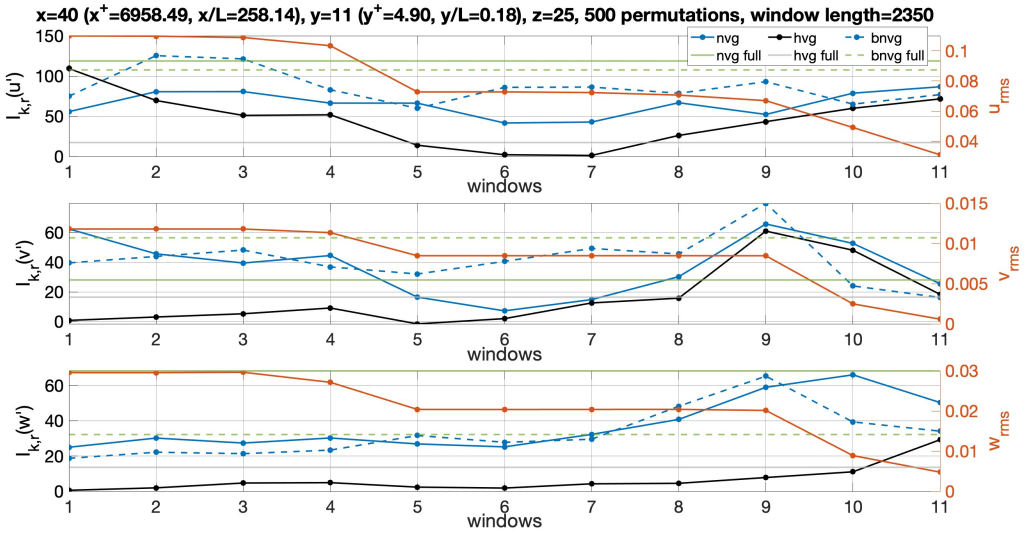

Figure 5.22: $I_{k,r}$ calculated by constant length windows (identified in fig. 5.21) and for the whole signal, compared to turbulent fluctuations for the three components of the fluctuations. NVG, HVG and BNVG are compared.

in its entirety. As before, the windows move forward each 235 time steps.

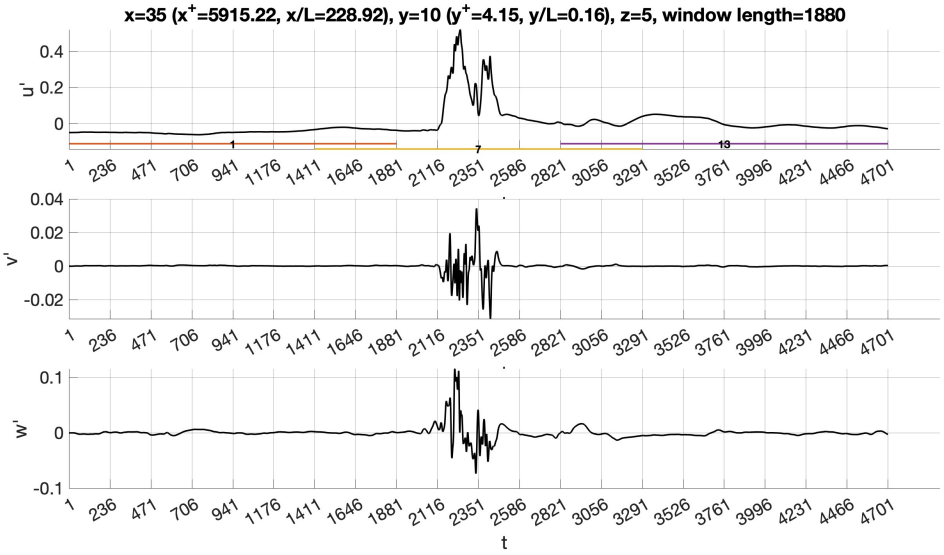

Figure 5.23: Time series of the fluctuations of the velocity. Windows' length is 1880 and they move every 235 time steps. Three different time windows are highlighted in different colours as an example of same-length windows.

In addition to what has already been observed in the previous signal, this case

presents interesting peaks of $I_{k,r}$ on windows number 3 and 11 in figure 5.24, that is those windows that we have previously defined as "entering" and "exiting" the spot. This fact is thereby substantiating the hypothesis that the most irreversible zones within the transition are precisely those transitions between the laminar and turbulent intervals of the signal.

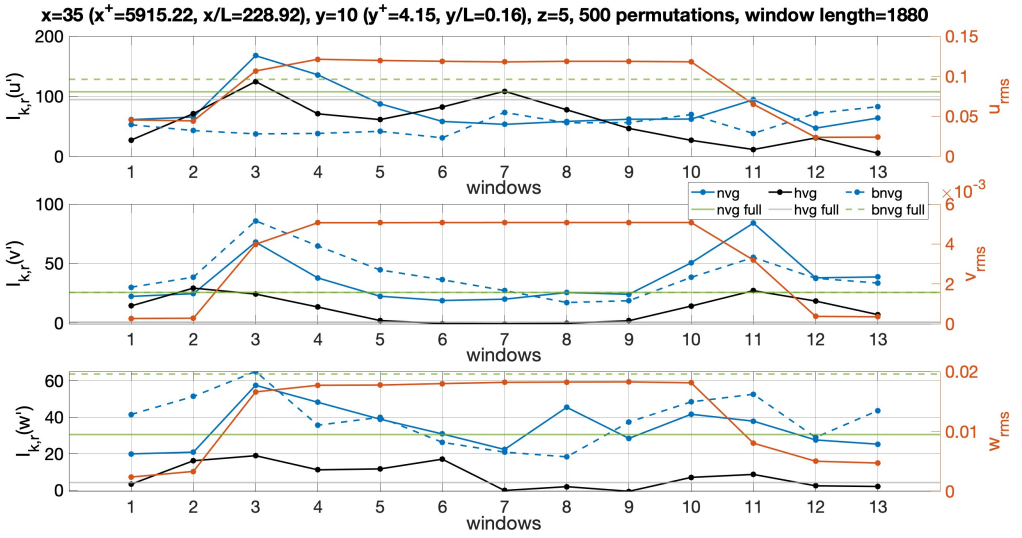

Figure 5.24: $I_{k,r}$ calculated by constant length windows (identified in fig. 5.23) and for the whole signal, compared to turbulent fluctuations for the three components of the fluctuations. NVG, HVG and BNVG are compared.

Sensitivity analysis on laminar signals length

Another investigation has been conducted to test the sensibility of the windows length when considering laminar parts of the signal. The method has been then applied on a window of variable length, starting from the whole signal and shrinking it by 100 time steps to the right and 100 to the left. The objective of this type of analysis is to investigate the suspected high values of $I_{k,r}$ in laminar signal ranges identified in the previous analyses.

The following three cases were considered:

- a signal in the transition zone (same as in figure 5.23),
- one in the laminar zone at a low x coordinate (figure 5.26),
- one in the turbulent zone at a high x coordinate(figure 5.28).

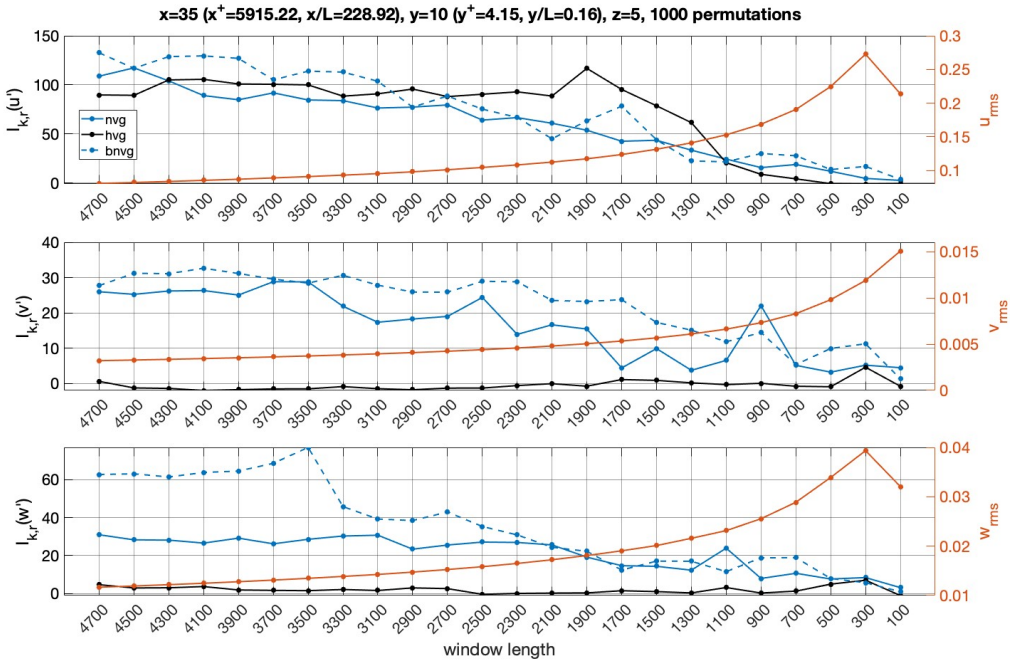

Figure 5.25: $I_{k,r}$ calculated by windows as their length decrease by 200 time steps at each point and compared to turbulent fluctuations for the three components of the fluctuations. NVG, HVG and BNVG are compared.

In all cases, regardless of whether the signal was extracted from a zone of laminar, intermittent or turbulent flow, the same behaviour has been obtained, that is, a decrease of $I_{k,r}$ as the length of the time window decreases (see figures 5.25, 5.27, 5.29). This helps to justify the fact that turbulent or transition signal segments presented lower values of $I_{k,r}$ than laminar ones, because the latter ones have always been analysed on longer time windows.

The significance of signal length (already mentioned in the previous paragraphs) in influencing the efficacy of the method is then confirmed, thereby validating the use of a fixed time window as previously outlined.

5.2.4 Generalisation on all signals

The next step, given the interesting results obtained, would be to generalize the analysis for all signals at all x, y and z. The problem becomes how to identify the right lengths for the time windows and how to analyse them without observing each signal individually, but with a method that can be general regardless of the

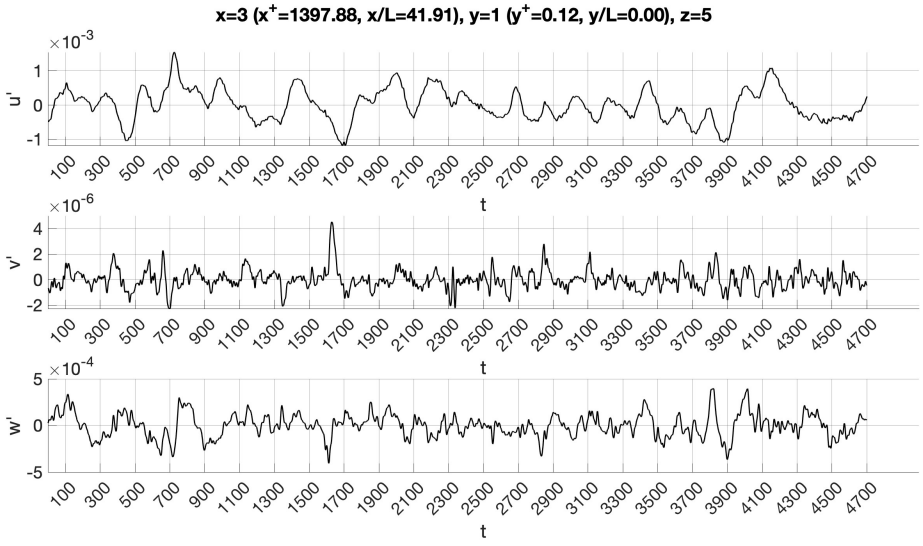

Figure 5.26: Signals of three components of the turbulent fluctuations for a point in the laminar zone.

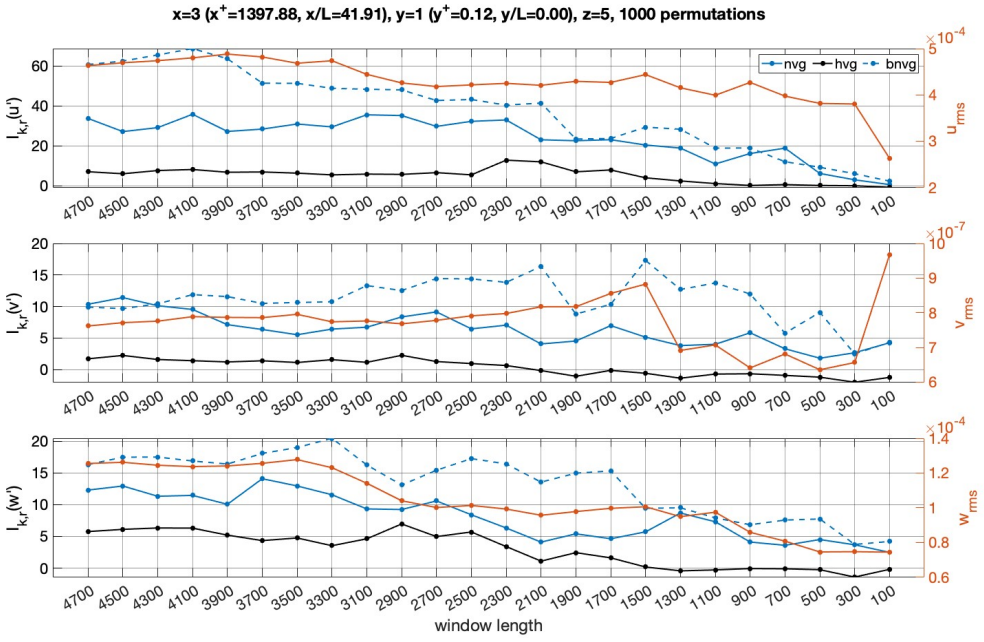

Figure 5.27: $I_{k,r}$ calculated by windows as their length decrease by 200 time steps at each point and compared to turbulent fluctuations for the three components of the fluctuations. NVG, HVG and BNVG are compared.

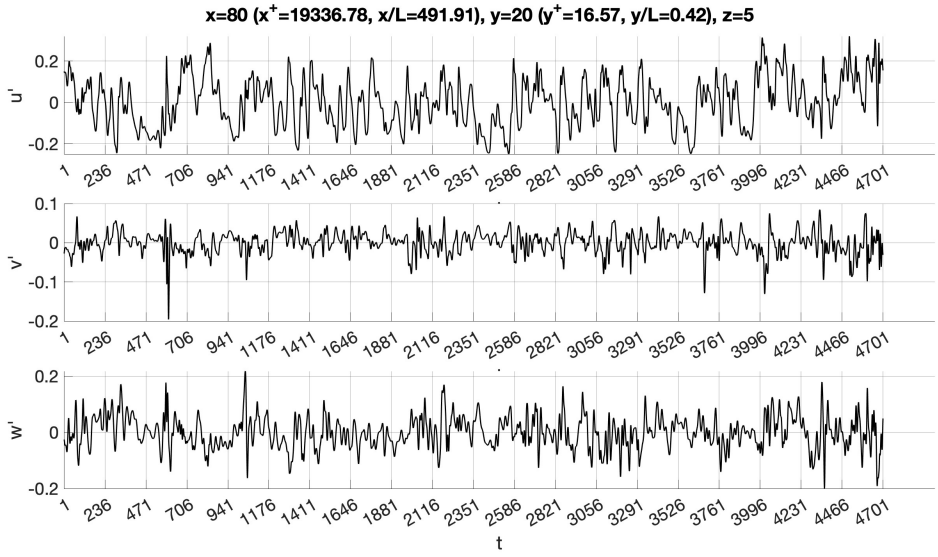

Figure 5.28: Signals of three components of the turbulent fluctuations for a point in the turbulent zone.

morphology of the signals, or regardless of the number and intensity of turbulent spots, that randomly develop throughout the boundary layer.

A first step in this sense has been made by trying to implement a method able to account for the intermittency of the signal and to count the turbulent spots, taking inspiration from the research of Hedley and Keffer [54].

A method for turbulent/non-turbulent decisions in an intermittent flow

Among many studies for the identification of the turbulent/non-turbulent interface in intermittent flows [53, 55, 56, 57, 58, 59], the one from Hedley and Keffer [54] provides and easy and straightforward method to identify turbulent regions in an intermittent signal. Here their research has been adapted to our intents; the following implementation adds to the original algorithm steps 3 and 4 that allow to calculate the number of spots and to fill the gaps in the indicator function.

1. Definition of a Turbulent/Non-Turbulent detection function: a binary indicator function $I(t)$ is constructed, defined as $I(t) = 1$ if the flow is turbulent, $I(t) = 0$ if it is non-turbulent.

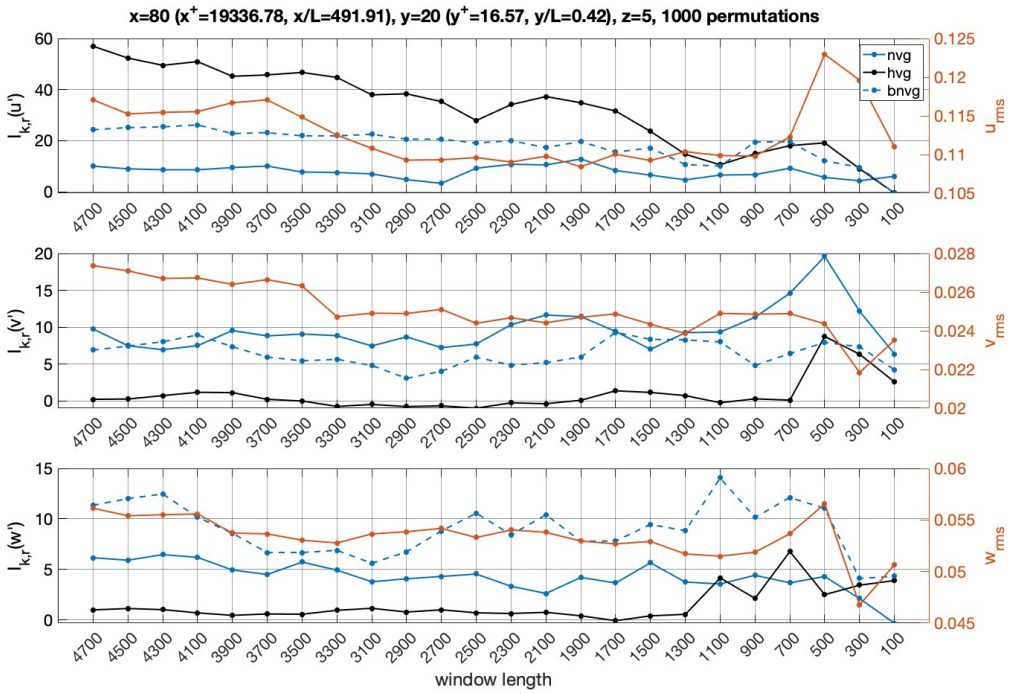

Figure 5.29: $I_{k,r}$ calculated by windows as their length decrease by 200 time steps at each point and compared to turbulent fluctuations for the three components of the fluctuations. NVG, HVG and BNVG are compared.

This classification is based on two criterion functions: $S(t)$, obtained by computing and smoothing $(du/dt)^2$ and $S_0(t)$, computed similarly with $(d^2u/dt^2)^2$, to enhance sensitivity to high gradients. It has to be noted that the criterion functions are not global, but strictly depend on the single signal. The binary decision rule is:

$$I(t) = \begin{cases} 1 & \text{if } S(t) > C \text{ or } S_0(t) > C_0 \\ 0 & \text{otherwise} \end{cases}$$

where C is the primary threshold, and $C_0 = C/C_{ratio}$ is the secondary threshold, typically with $C_{ratio} \simeq 0.3$, the value that has also been chosen in our adaptation.

2. Automatic selection of the optimal threshold: to avoid an arbitrary selection, the optimal threshold is estimated by means of an automatic algorithm based on the stability of the intermittency of the signal, $\gamma(C)$, which is defined as the fraction of time for which $I(t) = 1$.

The optimal threshold C^* is selected where the derivative $d\gamma/dC$ reaches a minimum, indicating a region where the indicator is stable with respect to small changes in threshold. Again, the choice of C^* depends on the signal. Alternatively, a minimum desired value for γ, or a maximum allowed threshold C, can be imposed to prevent unrealistically high threshold values.

3. Counting of the number of turbulent spots: once $I(t)$ has been computed, the number of turbulent spots, i.e. contiguous regions where $I = 1$, is determined by counting the number of transitions from 0 to 1:

$$N_{\text{spot}} = \sum_k [I(t_k) - I(t_{k-1}) = 1]$$

4. Merging of the turbulent spots separated by short gaps: to prevent short sequences of zeros from splitting a single spot into multiple fragments, a temporal filter is applied. This filter merges two turbulent regions if the number of zero-valued samples between them is less than or equal to a threshold, that in this case has been set to 90 time steps. This post-processing step enhances the robustness of spot identification in the presence of weak signal fluctuations.

As an example, the algorithm has been applied to one of the signals analysed previously: in figure 5.30 the criterion functions and the two indicator functions (before and after the filtering) are shown, together with the original signal $v'(t)$.

Through this method it has been possible to quantify the number of spots and locate them within the domain as depicted in figure 5.31 for the z-averaged values on the $x^+ - y^+$ plane and in figure 5.32 for two values of z on the plane. It is immediately evident that the areas with the greatest number of spots correspond to those outside the transition zone, that is to say to the laminar and fully turbulent flow regions. This is because, in these regions, the signals do not actually present proper turbulent spot, rather they are constituted by quite homogeneous signals in terms of fluctuations, resulting in a higher number of spots recognised by the algorithm. It is in fact at the onset of the transition zone that a limited number of spots can be observed, that is precisely where they start to develop, hence where the signals start to become more and more intermittent. Approaching the end of the transition zone, spots merge to form again more homogeneous - but very fluctuating - signals, hence explaining the increasing of the number of fluctuating regions in the signals. From a direct comparison with the values of $I_{k,r}$, the areas

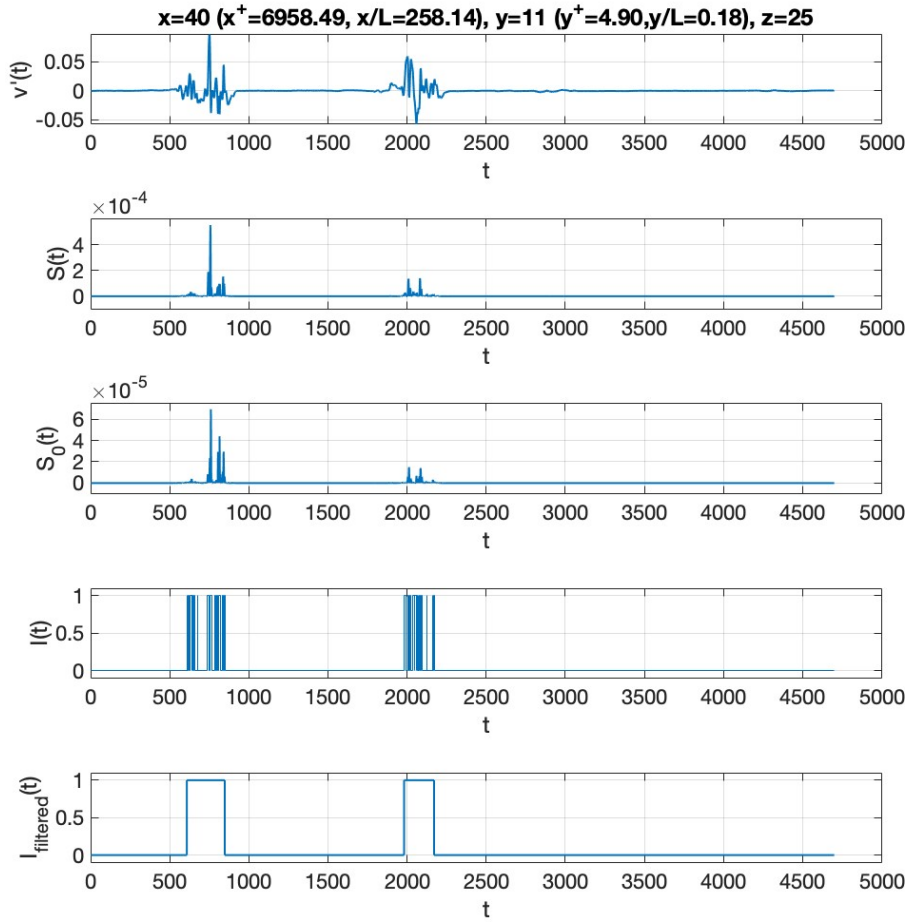

Figure 5.30: Application of the Hedley and Keffer inspired algorithm to a signal belonging to the transition zone, which exhibit two spots. From the top: the signal $v'(t)$, the criterion functions $S(t)$ and $S_0(t)$, the indicator functions $I(t)$ and $I_{filtered}(t)$.

previously identified as more irreversible correspond to the regions with the least number of spots, confirming the idea of a possible spot-irreversibility correlation stated in the last few paragraphs.

This is an efficient first step to finally relate time irreversibility to the turbulent structures characterizing the transitional boundary layer.

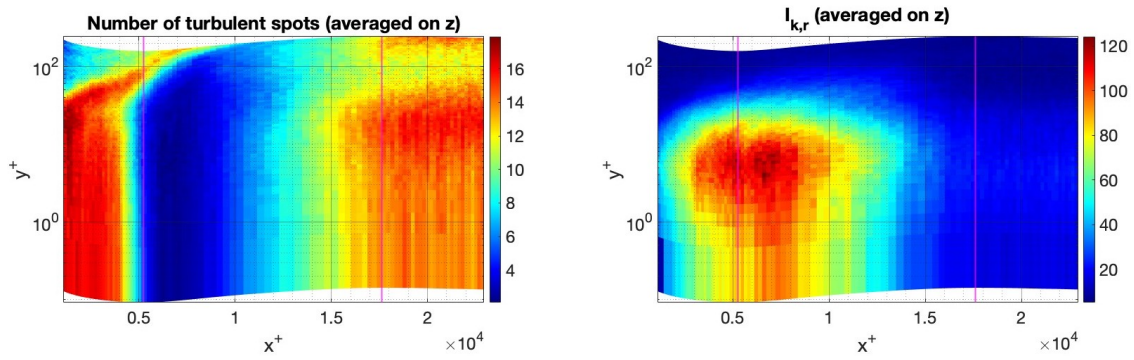

Figure 5.31: Comparison of the number of turbulent spots with the irreversibility ratio $I_{k,r}$ averaged on z on the $x^+ - y^+$ plane.

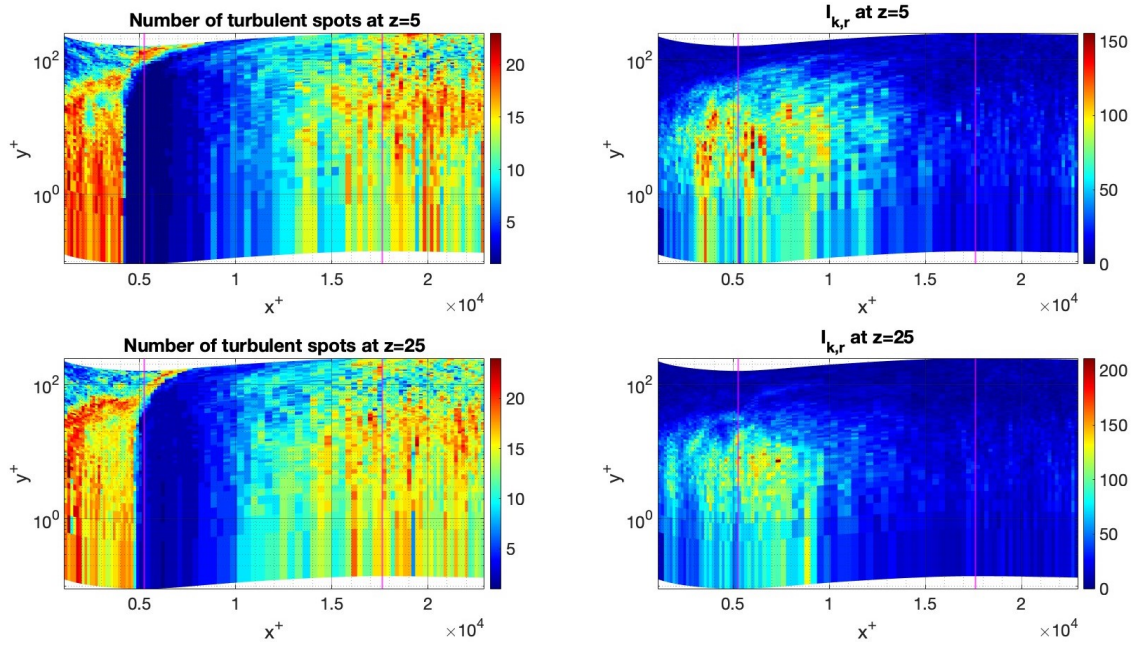

Figure 5.32: Comparison of the number of turbulent spots with the irreversibility ratio $I_{k,r}$ on the $x^+ - y^+$ plane for two values of the z coordinate.

5.3 Next studies: correlation between the turbulent spot and irreversibility

An optimal way to conclude this study would be to complete the previous algorithm with a stratagem to observe each and every spot evolution - its development from the laminar signal, its growth along the x coordinate in the boundary layer until its merging with other spots into a completely turbulent signal, how its 'in' and

'out' regions change and behave with respect to the rest of the signal - in a more automatic way, and correlate it to the results here achieved in the study of time irreversibility represented by measures I_k and $I_{k,r}$.

Chapter 6

Conclusions

The present work has explored the time irreversibility in a transitional boundary layer, with the aim of identifying the regions where temporal asymmetry emerges and understanding its connection to the underlying turbulent structures.

Using data from the JHTDB database and applying both the Horizontal and Natural Visibility Graph (HVG and NVG) method, the time series of the velocities have been transformed into graphs, allowing the computation of irreversibility by means of the Kullback-Leibler divergence between in- and out-degree probability distributions of the nodes associated to each point of the time series.

The results have revealed that time irreversibility is strongly localised in space and correlates with the transition zone and areas close to the wall, especially in the buffer layer. These are the regions mostly characterised by an intermittent behaviour and strong velocity fluctuations. Nonetheless, it has been shown that irreversibility does not directly depend on the amplitude of the fluctuations, rather it is driven by the temporal asymmetry and geometrical features of the signals, especially at the interface between their laminar and turbulent segments.

A local analysis carried out using moving temporal windows, in fact, has highlighted how irreversibility tends to reach higher values in transitional segments of the signals, rather than in fully developed turbulent or laminar ones. This supports the hypothesis that time irreversibility is linked to the coexistence and interaction of coherent structures of the boundary layer, such as streaks and turbulent spots. The analysis has also underlined the robustness and limitations of the visibility

graph method when applied to short signals, suggesting the need for complementary techniques or longer data windows in future works.

Overall, the study demonstrates that time irreversibility could act as an indication to detect transitional regimes and understand the turbulence onset mechanisms. The use of visibility graphs provides an innovative framework to connect time-series analysis and complex network theory in the context of fluid dynamics.

Future developments could include an extension of the analysis to spatio-temporal dynamics, in particular focusing on the evolution of each single turbulent spot and its contribution to the global irreversibility of the flow. Additionally, the adoption of more efficient spot detection algorithms could further enhance the precision and interpretability of the results, contributing to the understanding and theoretical modeling of turbulent transition.

Bibliography

[1] H. Xu, A. Pumir, and E. Bodenschatz, «Lagrangian view of time irreversibility of fluid turbulence», *Sci. China Phys. Mech. Astron.*, vol. 59, fasc. 1, p. 614702, 2016, doi: 10.1007/s11433-015-5736-x.

[2] G. Weiss, «Time-reversibility of linear stochastic processes», *Journal of Applied Probability*, vol. 12, fasc. 4, pp. 831–836, 1975, doi: 10.2307/3212735.

[3] A. J. Lawrance, «Directionality and Reversibility in Time Series», *International Statistical Review / Revue Internationale de Statistique*, vol. 59, fasc. 1, p. 67, 1991, doi: 10.2307/1403575.

[4] L. Lacasa, A. Nuñez, É. Roldán, J. M. R. Parrondo, and B. Luque, «Time series irreversibility: a visibility graph approach», *Eur. Phys. J. B*, vol. 85, fasc. 6, p. 217, 2012, doi: 10.1140/epjb/e2012-20809-8.

[5] L. Lacasa and R. Flanagan, «Time reversibility from visibility graphs of non-stationary processes», *Phys. Rev. E*, vol. 92, fasc. 2, p. 022817, 2015, doi: 10.1103/PhysRevE.92.022817.

[6] R. Kawai, J. M. R. Parrondo, and C. V. Den Broeck, «Dissipation: The Phase-Space Perspective», *Phys. Rev. Lett.*, vol. 98, fasc. 8, p. 080602, 2007, doi: 10.1103/PhysRevLett.98.080602.

[7] J. M. R. Parrondo, C. V. D. Broeck, and R. Kawai, «Entropy production and the arrow of time», *New J. Phys.*, vol. 11, fasc. 7, p. 073008, 2009, doi: 10.1088/1367-2630/11/7/073008.

[8] É. Roldán and J. M. R. Parrondo, «Estimating Dissipation from Single Stationary Trajectories», *Phys. Rev. Lett.*, vol. 105, fasc. 15, p. 150607, 2010, doi: 10.1103/PhysRevLett.105.150607.

[9] C. S. Daw, C. E. A. Finney, and M. B. Kennel, «Symbolic approach for measuring temporal "irreversibility"», *Phys. Rev. E*, vol. 62, fasc. 2, pp. 1912–1921, 2000, doi: 10.1103/PhysRevE.62.1912.

[10] É. Roldán and J. M. R. Parrondo, «Entropy production and Kullback-Leibler divergence between stationary trajectories of discrete systems», *Phys. Rev. E*, vol. 85, fasc. 3, p. 031129, 2012, doi: 10.1103/PhysRevE.85.031129.

[11] U. Frisch, Turbulence: The Legacy of A.N. Kolmogorov, 1ª ed. *Cambridge University Press*, 1995. doi: 10.1017/CBO9781139170666.

[12] S. B. Pope, *Turbulent flows*, Cambridge Univ. Press, 2015.

[13] T. A. Zaki, «From Streaks to Spots and on to Turbulence: Exploring the Dynamics of Boundary Layer Transition», *Flow Turbulence Combust*, vol. 91, fasc. 3, pp. 451–473, 2013, doi: 10.1007/s10494-013-9502-8.

[14] C. Lee and X. Jiang, «Flow structures in transitional and turbulent boundary layers», *Physics of Fluids*, vol. 31, fasc. 11, 111301, 2019, doi: 10.1063/1.5121810.

[15] J. Jucha, H. Xu, A. Pumir, and E. Bodenschatz, «Time-reversal-symmetry Breaking in Turbulence», *Phys. Rev. Lett.*, vol. 113, fasc. 5, p. 054501, 2014, doi: 10.1103/PhysRevLett.113.054501.

[16] T. D. Drivas, «Turbulent Cascade Direction and Lagrangian Time-Asymmetry», *J. Nonlinear Sci.*, vol. 29, fasc. 1, pp. 65–88, 2019, doi: 10.1007/s00332-018-9476-8.

[17] M. D. Pietro, L. Biferale, G. Boffetta, and M. Cencini, «Time irreversibility in reversible shell models of turbulence», *Eur. Phys. J. E*, vol. 41, fasc. 4, p. 48, 2018, doi: 10.1140/epje/i2018-11655-2.

[18] A. Cheminet et al., «Eulerian vs Lagrangian Irreversibility in an Experimental Turbulent Swirling Flow», *Phys. Rev. Lett.*, vol. 129, fasc. 12, p. 124501, 2022, doi: 10.1103/PhysRevLett.129.124501.

[19] G. Iacobello, L. Ridolfi, and S. Scarsoglio, «Large-to-small scale frequency modulation analysis in wall-bounded turbulence via visibility networks», *J. Fluid Mech.*, vol. 918, p. A13, 2021, doi: 10.1017/jfm.2021.279.

[20] G. Iacobello, S. Chowdhuri, L. Ridolfi, L. Rondoni, and S. Scarsoglio, «Coherent structures at the origin of time irreversibility in wall turbulence», *Commun Phys*, vol. 6, fasc. 1, p. 91, 2023, doi: 10.1038/s42005-023-01215-y.

[21] L. Lacasa, B. Luque, F. Ballesteros, J. Luque, and J. C. Nuño, «From time series to complex networks: The visibility graph», *Proc. Natl. Acad. Sci. U.S.A.*, vol. 105, fasc. 13, pp. 4972–4975, 2008, doi: 10.1073/pnas.0709247105.

[22] B. Luque, L. Lacasa, F. Ballesteros, and J. Luque, «Horizontal visibility graphs: Exact results for random time series», *Phys. Rev. E*, vol. 80, fasc. 4, p.

046103, 2009, doi: 10.1103/PhysRevE.80.046103.

[23] R. Flanagan and L. Lacasa, «Irreversibility of financial time series: A graph-theoretical approach», *Physics Letters A*, vol. 380, fasc. 20, pp. 1689–1697, 2016, doi: 10.1016/j.physleta.2016.03.011.

[24] J. F.Donges, R. V. Donner, and J. Kurths, «Testing time series irreversibility using complex network methods», *EPL*, vol. 102, fasc. 1, p. 10004, 2013, doi: 10.1209/0295-5075/102/10004.

[25] G. Iacobello, S. Scarsoglio, and L. Ridolfi, «Visibility graph analysis of wall turbulence time-series», *Physics Letters A*, vol. 382, fasc. 1, pp. 1–11, 2018, doi: 10.1016/j.physleta.2017.10.027.

[26] G. Iacobello, L. Ridolfi, and S. Scarsoglio, «A review on turbulent and vortical flow analyses via complex networks», *Physica A: Statistical Mechanics and its Applications*, vol. 563, p. 125476, 2021, doi: 10.1016/j.physa.2020.125476.

[27] D. Perrone, L. Ridolfi, and S. Scarsoglio, «Visibility analysis of boundary layer transition», *Physics of Fluids*, vol. 34, fasc. 10, p. 104104, 2022, doi: 10.1063/5.0106455.

[28] R. G. Jacobs and P. A. Durbin, «Simulations of bypass transition», *J. Fluid Mech.*, vol. 428, pp. 185–212, 2001, doi: 10.1017/S0022112000002469.

[29] A. Vela-Martín and J. Jiménez, «Entropy, irreversibility and cascades in the inertial range of isotropic turbulence», *J. Fluid Mech.*, vol. 915, p. A36, 2021, doi: 10.1017/jfm.2021.105.

[30] L. F. Richardson and P. Lynch, *Weather Prediction by Numerical Process*, 2ª ed. Cambridge University Press, 2007. doi: 10.1017/CBO9780511618291.

[31] Y. S. Kachanov, «Physical Mechanisms of Laminar-Boundary-Layer Transition», *Annu. Rev. Fluid Mech.*, vol. 26, fasc. 1, pp. 411–482, and 1994, doi: 10.1146/annurev.fl.26.010194.002211.

[32] R. Narasimha, «Modelling the Transitional Boundary Layer», *NASA Contractor Report 187487*, ICASE Report No. 90-90, NASA Langley Research Center, Hampton, VA, 1990.

[33] O. Vermeersch and D. Arnal, «Klebanoff-Mode Modeling and Bypass-Transition Prediction», *AIAA Journal*, vol. 48, fasc. 11, pp. 2491–2500, 2010, doi: 10.2514/1.J050002.

[34] T. A. Zaki and P. A. Durbin, «Mode interaction and the bypass route to transition», *J. Fluid Mech.*, vol. 531, pp. 85–111, 2005, doi: 10.1017/S0022112005003800.

[35] R. G. Jacobs and P. A. Durbin, «Shear sheltering and the continuous spectrum of the Orr–Sommerfeld equation», *Physics of Fluids*, vol. 10, fasc. 8, pp. 2006–2011, 1998, doi: 10.1063/1.869716.

[36] Lord Rayleigh, «On the Stability, or Instability, of certain Fluid Motions», *Proceedings of the London Mathematical Society*, vol. s1-11, fasc. 1, pp. 57–72, 1879, doi: 10.1112/plms/s1-11.1.57.

[37] M. T. Landahl, «A note on an algebraic instability of inviscid parallel shear flows», *J. Fluid Mech.*, vol. 98, fasc. 2, pp. 243–251, 1980, doi: 10.1017/S0022112080000122.

[38] L. Brandt, «The lift-up effect: the linear mechanism behind transition and turbulence in shear flows», *European Journal of Mechanics - B/Fluids*, vol. 47, pp. 80–96, 2014, doi: 10.1016/j.euromechflu.2014.03.005.

[39] X. Wu, R. G. Jacobs, J. C. R. Hunt, and P. A. Durbin, «Simulation of boundary layer transition induced by periodically passing wakes», *J. Fluid Mech.*, vol. 398, pp. 109–153, 1999, doi: 10.1017/S0022112099006205.

[40] L. Brandt and D. S. Henningson, «Transition of streamwise streaks in zero-pressure-gradient boundary layers», *J. Fluid Mech.*, vol. 472, pp. 229–261, 2002, doi: 10.1017/S0022112002002331.

[41] L. Brandt, «Numerical studies of the instability and breakdown of a boundary-layer low-speed streak», *European Journal of Mechanics - B/Fluids*, vol. 26, fasc. 1, pp. 64–82, 2007, doi: 10.1016/j.euromechflu.2006.04.008.

[42] L. Jin and Z. Tamer, «Transitional Boundary Layer Data Set». Johns Hopkins Turbulence Databases, 2018. doi: 10.7281/T17S7KX8.

[43] G. Iacobello, "Fast Horizontal Visibility Graph (HVG) for MATLAB," MathWorks File Exchange. [Online]. https://uk.mathworks.com/matlabcentral/fileexchange/72889-fast-horizontal-visibility-graph-hvg-for-matlab [Accesso: 18-giu-2025]

[44] G. Iacobello, "Fast Natural Visibility Graph (NVG) for MATLAB," MathWorks File Exchange. [Online]. https://uk.mathworks.com/matlabcentral/fileexchange/70432-fast-natural-visibility-graph-nvg-for-matlab [Accesso: 18-giu-2025]

[45] M. B. Kennel, «Testing time symmetry in time series using data compression dictionaries», *Phys. Rev. E*, vol. 69, fasc. 5, p. 056208, 2004, doi: 10.1103/PhysRevE.69.056208.

[46] C. Diks, J. C. Van Houwelingen, F. Takens, and J. DeGoede, «Reversibility

as a criterion for discriminating time series», *Physics Letters A*, vol. 201, fasc. 2–3, pp. 221–228, 1995, doi: 10.1016/0375-9601(95)00239-Y.

[47] C. Cammarota and E. Rogora, «Time reversal, symbolic series and irreversibility of human heartbeat», *Chaos, Solitons & Fractals*, vol. 32, fasc. 5, pp. 1649–1654, 2007, doi: 10.1016/j.chaos.2006.03.126.

[48] M. Zanin and D. Papo, «Algorithmic Approaches for Assessing Multiscale Irreversibility in Time Series: Review and Comparison», *Entropy*, vol. 27, fasc. 2, p. 126, 2025, doi: 10.3390/e27020126.

[49] G. Iacobello, M. Marro, L. Ridolfi, P. Salizzoni, and S. Scarsoglio, «Experimental investigation of vertical turbulent transport of a passive scalar in a boundary layer: Statistics and visibility graph analysis», *Phys. Rev. Fluids*, vol. 4, fasc. 10, p. 104501, 2019, doi: 10.1103/PhysRevFluids.4.104501.

[50] N. Ahmadi, R. M. H. Besseling, and M. Pechenizkiy, «Assessment of visibility graph similarity as a synchronization measure for chaotic, noisy and stochastic time series», *Soc. Netw. Anal. Min.*, vol. 8, fasc. 1, p. 47, 2018, doi: 10.1007/s13278-018-0526-x.

[51] A. González-Espinoza, G. Martínez-Mekler, and L. Lacasa, «Arrow of time across five centuries of classical music», *Phys. Rev. Research*, vol. 2, fasc. 3, p. 033166, 2020, doi: 10.1103/PhysRevResearch.2.033166.

[52] R. Nartallo-Kaluarachchi et al., «Multilevel irreversibility reveals higher-order organization of nonequilibrium interactions in human brain dynamics», *Proc. Natl. Acad. Sci. U.S.A.*, vol. 122, fasc. 10, p. e2408791122, 2025, doi: 10.1073/pnas.2408791122.

[53] B. Rehill, E. J. Walsh, L. Brandt, P. Schlatter, T. A. Zaki, and D. M. McEligot, «Identifying Turbulent Spots in Transitional Boundary Layers», 2011.

[54] T. B. Hedley and J. F. Keffer, «Turbulent/non-turbulent decisions in an intermittent flow», *J. Fluid Mech.*, vol. 64, fasc. 4, pp. 625–644, 1974, doi: 10.1017/S0022112074001832.

[55] D. Veerasamy and C. Atkin, «A rational method for determining intermittency in the transitional boundary layer», *Exp Fluids*, vol. 61, fasc. 1, p. 11, 2020, doi: 10.1007/s00348-019-2856-5.

[56] J. Lee and T. A. Zaki, «Detection algorithm for turbulent interfaces and large-scale structures in intermittent flows», *Computers & Fluids*, vol. 175, pp. 142–158, 2018, doi: 10.1016/j.compfluid.2018.08.015.

[57] N. Otsu, «A Threshold Selection Method from Gray-Level Histograms»,

IEEE Trans. Syst., Man, Cybern., vol. 9, fasc. 1, pp. 62–66, 1979, doi: 10.1109/TSMC.1979.4310076.

[58] D. H. Zhang, Y. T. Chew, and S. H. Winoto, «A proposed intermittency measurement method for transitional boundary layer flows», *Experiments in Fluids*, vol. 19, fasc. 6, pp. 426–428, 1995, doi: 10.1007/BF00190260.

[59] C. L. Kuan and T. Wang, «Investigation of the intermittent behavior of transitional boundary layer using a conditional averaging technique», *Experimental Thermal and Fluid Science*, vol. 3, fasc. 2, pp. 157–173, 1990, doi: 10.1016/0894-1777(90)90084-K.

Appendix A

Linear theory of stability

The evolution of a small perturbation in a parallel shear flow is governed by the Orr-Sommerfeld and Squire equations for wall-normal velocity v' and vorticity η' [13]:

$$\partial_t \begin{bmatrix} v' \\ \eta' \end{bmatrix} = \begin{bmatrix} \Delta^{-1}\left\{d_y^2 U\partial_x + (R^{-1}\Delta - U\partial_x)\,\Delta\right\} & 0 \\ -d_y U\partial_z & R^{-1}\Delta - U\partial_x \end{bmatrix} \begin{bmatrix} v' \\ \eta' \end{bmatrix}$$

where $U(y)$ is the mean flow profile, R is the Reynolds number, Δ is the Laplacian operator and Δ^{-1} its formal inverse.

We look for the modal solutions of equations, by assuming that the flow is homogeneous in the streamwise and spanwise directions. This allows us to use a Fourier representation of the perturbations in these directions and in time:

$$\begin{bmatrix} v'(x,t) \\ \eta'(x,t) \end{bmatrix} = \begin{bmatrix} \phi(y) \\ \chi(y) \end{bmatrix} e^{i(k_x x + k_z z - \omega t)}$$

where $\phi(y)$ and $\chi(y)$ are the wall-normal velocity and vorticity eigenfunction, respectively, k_x and k_z are the streamwise and spanwise wavenumbers, ω is a frequency representing the growth rate.

We can then write an eigenvalue problem to solve for the complex frequency ω and the associated eigenfunctions $\phi(y)$ and $\chi(y)$:

$$-i\omega \begin{bmatrix} \phi(y) \\ \chi(y) \end{bmatrix} = \begin{bmatrix} \mathcal{L} & 0 \\ -\mathcal{C} & \mathcal{S} \end{bmatrix} \begin{bmatrix} \phi(y) \\ \chi(y) \end{bmatrix}$$

with

$$\mathcal{L} = \Delta^{-1}\left\{ik_x U'' + [\Delta(\Delta)/R] - ik_x U\Delta\right\}$$

$$\mathcal{S} = [\Delta/R - ik_x U]$$

$$\mathcal{C} = ik_z U'$$

In the case of boundary layers, the eigenspectrum of Orr–Sommerfeld and Squire equations is divided into discrete and continous components. The former is constituted by a finite set of eigenvalues ω_n, whose associated modes $\phi_n(y)$ and $\chi_n(y)$ are located in the boundary layer and decay in the free-stream [13]. These are usually associated to classical instabilities such as Tollmien-Schlichting waves and represent the main mechanisms of orderly transition to turbulence.

The continous component correspond to a continous set of eigenvalues ω_{k_y}, parametrised by a transversal wavenumber k_y. These modes are oscillatory in the free-stream, where they resemble Fourier modes, but decay towards the boundary layer wall. The penetration depth of each mode depends on its frequency, wavenumber, local Reynolds number and local shear [34], explaining, in a way, the concept of shear sheltering and how the continous branch of modes plays a fundamental role in the bypass transition.